

This manuscript is a preprint. It has been submitted to a special issue of *Frontiers in Earth Science*. Subsequent versions of this manuscript may have different content. If accepted, the final version of this manuscript will be available via the 'Peer reviewed Publication DOI' link via this webpage. We welcome feedback, so please feel free to contact any of the authors directly or to comment on the manuscript.

Displacement/length scaling relationships for normal faults; a review, critique, and revised compilation

Lathrop, B. A. ¹, Jackson, C. A-L. ², Bell, R. E. ¹, & Rotevatn, A. ³

¹ Basins Research Group (BRG), Department of Earth Science & Engineering, Imperial College, Prince Consort Road, London, SW7 2BP

² Department of Earth and Environmental Sciences, University of Manchester, Williamson Building, Oxford Road, Manchester, M13 9PL, UK

³ Department of Earth Science, University of Bergen, PO Box 7800, 5020 Bergen, Norway

Corresponding author: Bailey Lathrop (b.lathrop17@imperial.ac.uk)

1 **Abstract**

2 The relationship between normal fault displacement (D) and length (L) varies due to
3 numerous factors, including fault size, maturity, basin tectonic history, and host rock
4 lithology. Understanding how fault D and L relate is useful, given related scaling laws are
5 often used to help refine interpretations of often incomplete, subsurface datasets, which has
6 implications for hydrocarbon and low-carbon energy applications. Here we provide a review
7 of D/L scaling laws for normal faults, discuss factors that could influence these relationships,
8 including both geological factors and errors in measurement, and provide a critique of
9 previously published D/L databases. We then present our newly assembled database of 4035
10 normal faults from 64 sources that include explicit information on: (i) fault length and
11 displacement, (ii) host rock lithology, (iii) host basin tectonic history, and (iv) maturity, as
12 well as fault D and L through time when these data are available. We find an overall scaling
13 law of $D=0.3L^{0.92}$, which is similar to previously published scaling equations and that varies
14 in response to the aforementioned geological factors. Our data show that small faults (<1 m
15 length) tend to be over-displaced compared to larger faults, active faults tend to be over-
16 displaced compared to inactive faults, and faults with stiffer host rock lithologies, like
17 volcanic and carbonate rocks, tend to be under-displaced with respect to faults within softer,
18 more compliant host rocks, like clastic sedimentary rocks. Our dynamic D/L through time
19 data show that faults follow the *hybrid fault growth* model, i.e., they initially lengthen, during
20 which time they will appear under-displaced, before accumulating displacement. To the best
21 of our knowledge, this is the first comprehensive, integrated, critical study of D/L scaling
22 laws for normal faults and the factors influencing their growth. These revised relationships
23 can now be utilized for predicting fault length or displacement when only one variable is
24 available and provide the basis for general understanding D/L scaling laws in the context of

25 normal fault growth. This underpinning database is open-access and is available for analysis
26 and manipulation by the broader structural geology community.

27

28 **3.1. Introduction**

29 The relationship between normal fault displacement (D) and length (L) has been widely
30 researched over several decades (e.g., Walsh & Watterson 1988; Cowie & Scholz 1992a;
31 Dawers et al., 1993; Clark and Cox, 1996; Schultz & Fossen, 2002; Kim & Sanderson, 2005;
32 Schultz et al., 2008; Torabi & Berg, 2011; Xu et al., 2006). The empirical relationship
33 between D and L is often described by:

34

$$35 \quad D_{max}=cL^n$$

36

37 The value n may range from 0.5 to 2.0 ($n=0.5$, Fossen & Hesthammer, 1997; $n=1$, Cowie &
38 Scholz, 1992a; Dawers et al., 1993; Scholz et al., 1993; Clark & Cox, 1996; Schlische et al.,
39 1996; Kim & Sanderson, 2005; Xu et al., 2006; $n=1.5$, Marrett & Allmendinger, 1991;
40 Gillespie et al., 1992; $n=2$, Watterson, 1986; Walsh & Watterson, 1988). $n=1$ indicates a
41 linear scaling law, which implies that faults of different sizes act similarly and $n \neq 1$ indicates a
42 scale-dependent geometry (Kim & Sanderson, 2005; Schultz et al., 2008).

43 The value c (sometimes written as P or γ) is an expression of fault displacement at and is
44 hypothesized to be related to rock material properties such as shear strength and elasticity, as
45 well as the driving stress; for example, as rock shear strength increases, for example from a
46 mudstone to a granite, c increases (Walsh & Watterson, 1988; Cowie & Scholz, 1992b;
47 Gillespie et al., 1992; Ackermann et al., 2001; Kim & Sanderson, 2005; Schultz et al., 2008;
48 Torabi & Berg, 2011). Reported values of c range from 0.0001-1 (Schulz et al., 2008; Torabi
49 & Berg, 2011), although they typically fall between 0.001 and 0.1 (Schultz et al., 2008;
50 Torabi & Berg, 2011). High values of c (i.e., $c=1$) have been documented from strike-slip
51 faults (MacMillan, 1975; Torabi & Berg, 2011).

52 This scaling relationship defined above has typically been used to: i) assess the way in which
53 normal faults form, with applications to geohazard analysis (Cowie & Scholz, 1992b), and ii)
54 allow better prediction of fault dimensions, with applications to energy resource exploration
55 and extraction, nuclear waste, and CO₂ storage, which all rely on robust structural models

56 that are commonly constructed from incomplete datasets (Torabi & Berg, 2011; Kolyukhin &
57 Torabi, 2012). We may need to estimate L when only D (or vice versa) can be observed in an
58 isolated field exposure or in a single 2D seismic reflection profile. For example, fault
59 connectivity impacts fluid flow from source to reservoir, thus knowing how fault length
60 might impact that, and how displacement may influence fault seal, is key when assessing the
61 resource potential of a sedimentary basin.

62 When plotted in log-log space, the relationship between displacement and length appears
63 strongly positively correlated across several orders of magnitude (see D/L plots in Walsh &
64 Watterson, 1998; Cowie & Scholz, 1992a; Schlische et al., 1996; Kim & Sanderson, 2005;
65 Torabi & Berg, 2011). However, the relationship between normal fault length and
66 displacement is highly variable, and a one-size-fits all equation to describe D/L scaling is
67 likely imprecise. Understanding how factors such as tectonic history, fault maturity, host rock
68 lithology, and fault size effect D/L scaling, and using these observations to create bespoke
69 D/L equations, will improve our ability to estimate either parameter.

70 D/L scaling relationships may not only describe the finite geometry of a normal fault, but
71 they may also provide insights into how faults grow. For example, a linear relationship (i.e.,
72 $n=1$) between D and L was used to justify a model of normal fault growth where faults
73 accumulated displacement and length synchronously; this was originally referred to as the
74 *isolated fault model*, but is now commonly referred to as the *propagating fault model* (e.g.,
75 Walsh & Watterson, 1988; Morley et al., 1990; Dawers et al., 1993; Cartwright et al., 1995;
76 Walsh et al., 2003; Childs et al., 2017b; Rotevatn et al., 2019). However, numerous studies
77 have since challenged the notion that fault growth follows a linear trajectory in D-L scaling
78 space and have instead argued that faults grow in accordance with the *constant-length model*,
79 i.e., faults reach their near-final length rapidly and then accrue displacement without
80 significant further tip propagation (e.g., Walsh et al., 2002, 2003; Nicol et al., 2005, 2017;
81 Jackson & Rotevatn, 2013; Henstra et al., 2015; Fossen & Rotevatn, 2016; Hemelsdaël &
82 Ford, 2016; Tvedt et al., 2016; Childs et al., 2017b; Rotevatn et al., 2019; Pan et al., 2021).
83 Faults have also been shown to grow in accordance with the *hybrid fault model*; this
84 combines the propagating and constant-length models, suggesting that faults grow in two
85 distinct phases: (i) an initial phase (20-30% of the faults life), when maximum fault length is
86 reached by segment tip propagation and linkage and 10-60% of displacement is accrued, (ii) a
87 second stage (the remaining 70-80% of the faults life) when 40-90% of displacement is
88 accrued (Rotevatn et al. 2019). Some faults may also experience a stage of lateral tip-line

89 retreat in the last ~25% of their lives, where slip is concentrated along their central portions
90 (Meyer et al., 2002; Morley 2002; Nicol et al., 2020; Lathrop et al., 2021).

91 Global compilations of D/L data result in a range of scaling relationships with different
92 values for both c and n . There are several possible reasons for this. First, these compilations
93 may contain faults with errors in measurement of D and/or L, resulting in scaling laws that
94 are not as reliable as we wish or need. Second, there has been little research into how D/L
95 scaling relationships change for faults: (i) of different size, (ii) forming in differing tectonic
96 settings (i.e., if a fault forms due to the reactivation of an older structure, or whether it is
97 newly formed in previously undeformed or only weakly deformed host rock), (iii) forming in
98 different host rock lithologies, and (iv) that have been active for different lengths of time (i.e.,
99 fault maturity, which may relate to whether a fault is in a tectonically active area or not). It
100 has been noted that these factors can cause high variability in global datasets (e.g., Cowie &
101 Scholz, 1992a; Nicol et al., 2010; Rotevatn et al., 2019), but this variability has not yet been
102 quantified (see section 2). Finally, if faults really do grow via a constant-length or hybrid
103 fault growth model, D/L ratios will vary greatly throughout the life of a fault, and thus D/L
104 ratios from faults of different stages in their development are less meaningful, and a
105 compilation of dynamic D/L data will more accurately show how faults grow than a single
106 measurement taken: (i) at the end of a fault's life, once it has become inactive, or (ii) as a
107 snapshot at a specific, possibly unknown time in the fault's development.

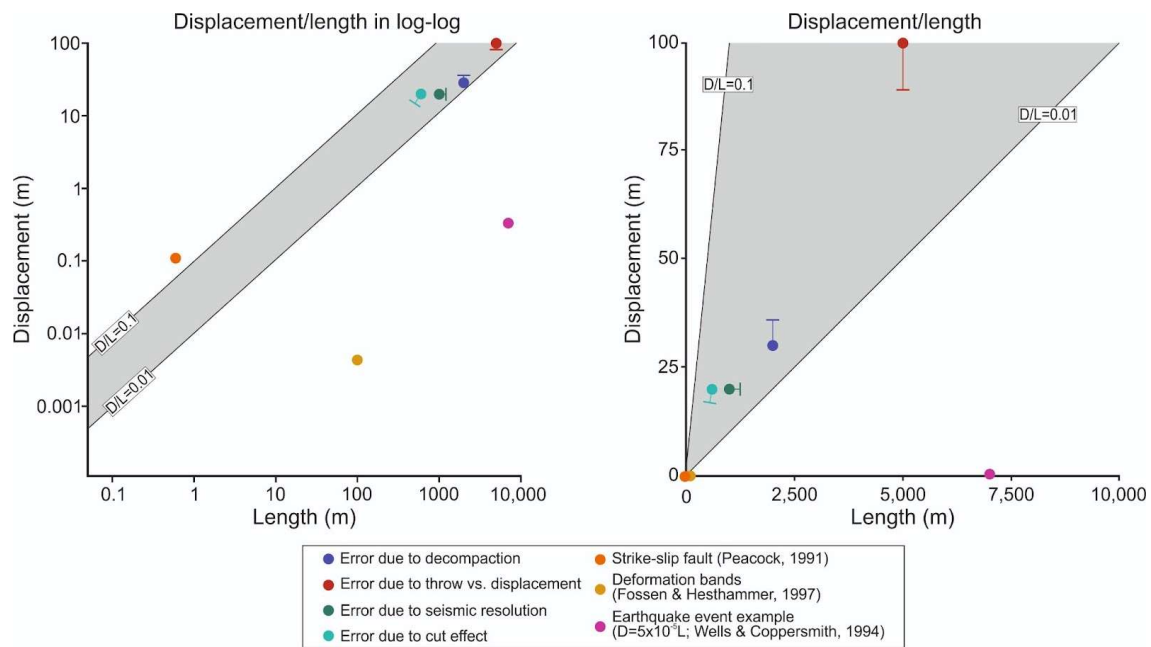
108 It is clear there are numerous factors that may cause variability in the important, widely used
109 relationship between normal fault displacement and length. In this paper we look closely at
110 these two parameters, isolating various factors that could affect the relationship between the
111 two, and proposing improved scaling laws for specific geological setting. We first summarise
112 and discuss inconsistencies in previous compilations of D and L, critically quality checking
113 the included data. We next provide a new open-source normal fault database that includes
114 factors such as fault maturity, tectonic history, and host rock lithology, which previous work
115 suggests may be important to consider when establishing and ultimately applying D/L
116 relationships. We also compile data on normal fault D and L through time (i.e., from
117 structures flanked by growth strata that permit displacement and length backstripping; Meyer
118 et al., 2002; Tvedt et al., 2016; Jackson et al, 2017; Lathrop et al., 2021; Pan et al., 2021,
119 physical analogue studies; Schlagenhauf et al., 2008; and numerical modelling studies; Finch
120 & Gawthorpe, 2017) to show how faults may grow and how D/L ratios may change through
121 time. Finally, we interrogate our new database and discuss how fault size, host rock lithology,

122 regional tectonic history, and fault maturity affect fault growth and D/L scaling. Our new
 123 database of normal fault properties demonstrates that one-size-fits-all scaling relationships
 124 are overly simplistic and that D/L scaling relationships should not be used indiscriminately.

125

126 3.2. How might geological factors and measurement errors influence 127 scaling laws?

128 There are a range of geologic phenomena that can cause normal faults to be over or under-
 129 displaced, and that are known to influence D/L scaling laws. Several common errors in
 130 measurement can also influence D/L scaling laws. We briefly outline these and illustrate how
 131 the related data would theoretically plot in D/L scaling space (Figure 1), before highlighting
 132 measurement errors in published datasets.



133

134 **Figure 1.** Schematic showing how errors in measurement and data from structures other than normal faults that
 135 can affect D/L scaling in and out of log-log space. Dots signify observed values and one-sided error bars
 136 delineate where the observed value should be.

137

138 3.2.1. Geological factors

139 Different geological phenomena could affect the relationship between fault length and
 140 displacement. Tectonic setting is said to affect the relationship between D and L (Cowie &
 141 Scholz, 1992a). Specifically, reactivated faults can establish their maximum length more
 142 quickly than non-reactivated faults, which means reactivated normal faults may have a

143 relatively low D/L ratio, at least in the early stages of their growth (Walsh et al., 2002, Vétel
144 et al., 2005, Baudon & Cartwright, 2008, Giba et al., 2012, Whipp et al., 2014).

145 The amount of time that a fault has been active can also affect D/L scaling. For example,
146 Mouslopoulou et al. (2009) note that fault displacement rates vary through time, especially
147 for ‘young’ faults (<20 Kyr), which can result in ~an order-of-magnitude scatter in D/L
148 scaling. Nicol et al. (2010) demonstrate that active faults are under-displaced in the early
149 stages of their growth, with the D/L ratio increasing with time (i.e., the constant-length fault
150 model, e.g., Walsh et al., 2002, 2003; Nicol et al., 2005; 2010, 2017; Rotevetn et al., 2019).

151 Host rock lithology can change the D/L ratio of a fault, with host rock lithology linked to
152 shear modulus and Young’s Modulus. Walsh & Watterson (1988, 1989), Cowie & Scholz
153 (1992b) and Wibberley et al. (1999) compare D/L scaling and host rock shear modulus,
154 showing that stiffer lithologies (i.e., high shear modulus) are under-displaced compared to
155 softer lithologies (i.e., low shear modulus). Agreeing with this, Gudmundsson et al. (2004)
156 notes that faults with a low Young’s Modulus and D/L are inversely related, i.e., faults within
157 softer and/or more deformed host rocks have a lower Young’s Modulus and higher D/L ratios
158 (over-displaced), whereas faults within stiffer host rocks have a higher Young’s Modulus and
159 lower D/L ratios (under-displaced). Several studies have also shown that mechanical
160 stratigraphy can affect D/L scaling (Muraoka & Kamata, 1983; Nicol et al., 1996; Gross et
161 al., 1997; Schulz & Fossen, 2002; Soliva et al., 2006; Roche et al., 2013, 2014). For example,
162 faults can be stratigraphically confined within stiffer layers, with bounding softer or more
163 compliant layers preventing faults from propagating vertically (but not laterally), and thus
164 causing them to be under-displaced (Schulz & Fossen, 2002).

165 Fault size could also affect D/L scaling, although there is some disagreement as to precisely
166 how. For example, Schlische et al. (1996) did not find a relationship between D/L and fault
167 size, although in contrast, Cowie & Scholz (1992a) found that large faults (>1 km of
168 displacement) are over-displaced compared to smaller faults, whereas Torabi & Berg (2011)
169 noted that small faults (<1 m of displacement) and large faults (>1 km of displacement) have
170 higher D/L ratios than medium faults (those with displacement between 1 m and 1 km).

171 When faults have along-fault changes in dip (i.e., fault dip changes in cross-section), strain,
172 typically in the form of folding, is partitioned onto bends; this may cause faults to appear
173 either over or under-displaced. According to estimates by Delokgos et al. (2020), fault bends
174 can cause throw to be under-estimated by approximately 10%, and up to 50% in extreme

175 cases. Related to this, fault drag can reduce the amount of displacement measured on a
176 normal fault, especially on large faults (Walsh & Watterson, 1987; Gross et al., 1997; Kim &
177 Sanderson, 2005; Childs et al., 2017a; Delogkos et al., 2017). Delogkos et al. (2017) noted
178 that fault drag accounted for up to ~24% of the total throw on faults with throws between 35-
179 550 m.

180 Igneous sill emplacement can also modify D/L scaling. For example, the inflation of an
181 igneous sill within the hangingwall of a pre-existing normal fault can cause reverse
182 reactivation of the fault, causing a decrease in fault displacement and in the ratio between D
183 and L. As a result, the fault geometry and related scaling relationship may not reflect the
184 fault's growth history (Norcliffe et al., 2021).

185 The growth of normal faults by linkage of segments can also cause faults to have multiple,
186 smaller displacement maxima, instead of a single, large maximum displacement value. This
187 can cause the faults to appear under-displaced (e.g., Peacock & Sanderson, 1991; Gillespie et
188 al., 1992; Cartwright et al., 1995; Dawers et al., 1995; Acocella et al., 2000; Xu et al., 2006;
189 Faure Walker et al., 2009).

190 **3.2.2. Measurement errors**

191 In addition to the geological factors outlined above, the relationship between displacement
192 and length could be affected by precisely where on a fault surface these values are measured,
193 i.e., it is possible that the true maximum length and displacement have not been recorded
194 (Kim & Sanderson, 2005; Torabi et al., 2019). Maximum displacement is typically located
195 near the fault centre, however an arbitrary section of the fault exposed in outcrop may not
196 pass through the centre, which is referred to as the 'cutting effect' (Kim & Sanderson, 2005).

197 If fault offset is measured as throw instead of displacement and is then included in a D/L
198 database without knowledge of fault dip, the D/L ratio would be inaccurate (Figure 1). This
199 does not greatly alter the position of a data point on a D-L plot (Figure 1), but it could affect
200 the derived scaling equations.

201 D/L ratios can be skewed if different types of faults are plotted together. For example, strike-
202 slip faults tend to be over-displaced compared to normal faults, with D/L ratios being as high
203 as 1:1, whereas normal faults have a maximum ratio of 1:2 (Kim & Sanderson, 2005; Torabi
204 & Berg, 2011), so this could skew normal fault scaling laws towards being more over-
205 displaced (Figure 1). The higher D/L ratios in this case are possibly due to fault length being

206 measured parallel to slip direction, whereas fault length should be measured perpendicular to
207 dip for a pure dip-slip normal fault (Kim & Sanderson, 2005; Torabi & Berg, 2011).

208 Displacement and length relationships measured from individual earthquakes scale
209 differently to those derived from faults, i.e., the average slip to rupture length scaling
210 relationship for individual earthquake events is $D=5 \times 10^{-5}L$ (Wells & Coppersmith, 1994;
211 Iezzi et al., 2018; Figure 1), thus data from individual earthquakes should not be added to D-
212 L scaling databases. D-L data derived from individual earthquakes record only the length
213 dimension of the slip patch and the magnitude of slip.

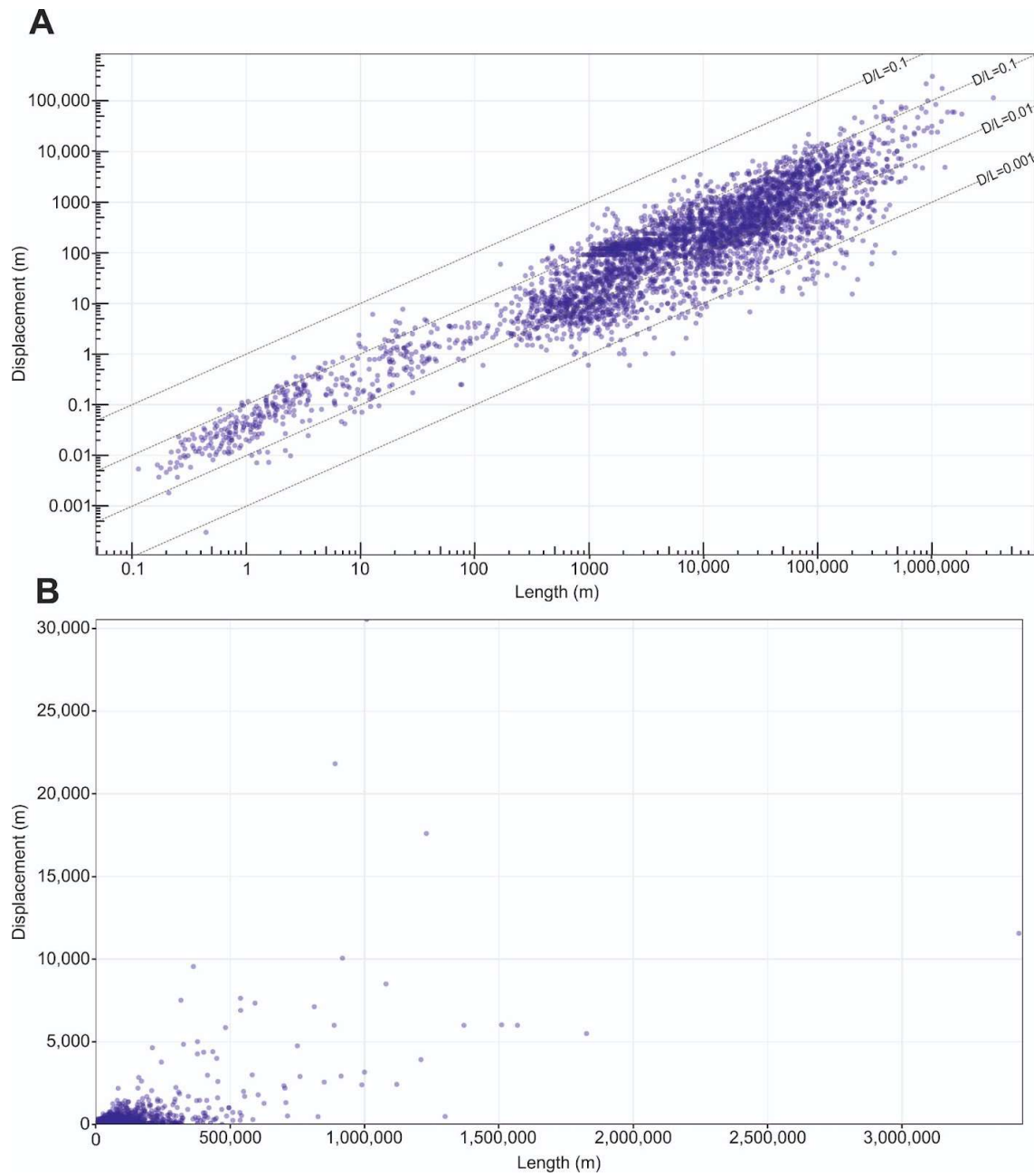
214 Deformation bands are mechanically different than tectonic faults; deformation bands
215 experience strain hardening after formation due to grain interlocking, with strain then tending
216 to localize elsewhere and form new bands instead of increasing displacement on existing
217 bands (Fossen & Rotevatn, 2012). This causes deformation bands to be under-displaced
218 compared to tectonic faults, usually having a value of $n=0.05$. Inclusion of deformation bands
219 in D/L scaling databases would thus skew D/L scaling relationships (Wibberly et al., 2000b;
220 Schulz et al., 2008; Fossen & Rotevatn, 2012; Figure 1).

221 There is also error associated with D/L measurements obtained from normal faults imaged in
222 3D seismic reflection data. For example, length could be underestimated by a few hundred
223 meters to a few kilometres, depending on fault size, due to the displacement near the fault tips
224 being under seismic resolution (Yielding et al., 1996; Pickering et al., 1997; Rotevatn &
225 Fossen, 2011). If fault displacement is measured in time- (rather than depth-) migrated
226 seismic reflection data, a good knowledge of subsurface velocities is needed to accurately
227 convert values of displacement in milliseconds two-way time (ms TWT) to metres. If these
228 velocity data are poor, there will be uncertainty around D, and the D/L ratio may accordingly
229 be inaccurate, i.e., if the applied velocity is too high, displacement, and the D-L ratio, will be
230 under-estimated. Compaction could also decrease throw values (up to 20% compaction
231 according to Taylor et al., 2008; Figure 1), which can be an issue for deeply buried faults in
232 compactable, mudstone-dominated host rock.

233 The measurement errors described above can visually skew plotted data and significantly
234 change calculated D/L scaling laws. D/L scaling laws are undoubtedly important for
235 attempting to estimate D from L (or vice-versa), but D/L plots are also important as they are
236 often used to qualitatively check if a D/L relationship is strong or weak. These errors can
237 skew D/L plots to different extents, depending on how the data are presented (Figure 1). The

238 effects of errors such as measuring throw instead of displacement, the cutting effect, the
239 impact of post-formation decompaction, and issues related to seismically imaging low-
240 displacement fault tips, result in changes that are apparent in a graph not presented in log-log
241 space (Figure 1a), but that make little difference in a log-log D/L graph (Figure 1b). Data in
242 log-log space tend to 'hide' fluctuations due to small measurement errors, as data will move
243 very little and will still lie within the range of values in the global database. These errors in
244 measurement could change D/L scaling laws, but unless the error is more than an order of
245 magnitude than the correct value, it likely will not be seen in log-log space. However, when
246 structures other than normal faults, such as strike-slip faults and deformation bands, or
247 measurements from singular earthquake events are included in a database, they fall
248 significantly outside the typical range of D/L values (Figure 1). While more error is visible in
249 a plot not in log-log space, there is a bias towards larger faults if the plot spans several orders
250 of magnitude, as only the largest faults are visible when faults of all sizes are included on one
251 plot (see Figure 1).

252



253

254 *Figure 2. Plots showing fault length vs displacement for all data in our database. A) Data in log-log space. B)*
 255 *Data not in log-log space.*

Database	# of faults	Sources Used	n	C
Walsh & Watterson, 1988	308	Beck, 1929; Reeves, 1929; Teas, 1929; Babenroth & Strahler, 1945; Brunstrom, 1963; Tschopp, 1967; Janoschek & Gotzinger, 1969; Mayuga, 1970; Bond et al., 1971; Huntoon, 1974; Cave, 1977; Shepherd & Burns, 1978; Shoemaker et al., 1978; Frost & Smart, 1979; Drozdowski, 1980; Frost & Halliday, 1980; Nelson, 1980; Van den Bark & Thomas, 1980; Verdier et al., 1980; Muroaka & Kamata, 1983; Aitkenhead et al., 1985	2	not given
Cowie & Scholz, 1992	210	MacMillan, 1975; Elliott, 1976; Muroaka & Kamata, 1983; Walsh & Watterson, 1987; Krantz, 1988; Opheim & Gudmusson, 1989; Peacock, 1991; Peacock & Sanderson, 1991; Villemin et al., 1995	1	0.006-0.17 (range)
Schlische et al., 1996	547	MacMillan, 1975; Elliott, 1976; Muroaka & Kamata, 1983; Walsh & Watterson, 1987; Krantz, 1988; Opheim & Gudmusson, 1989; Peacock, 1991; Peacock & Sanderson, 1991; McGrath, 1992; Dawers et al., 1993; Villemin et al., 1995	1.06	0.03 (average)
Bailey et al., 2005	9618	Beck, 1929; Reeves, 1929; Teas, 1929; Babenroth & Strahler, 1945; Fox, 1959; Brunstrom, 1963; Woodland & Evans, 1964; Tschopp, 1967; Janoschek & Gotzinger, 1969; Wood et al., 1969; Freund, 1970; Mayuga, 1970; Bond et al., 1971; MFRG, 1973; Huntoon, 1974; MacMillan, 1975; Elliott, 1976; Cave, 1977; Ruzhich, 1977; Shepherd & Burns, 1978; Frost & Smart, 1979; Drozdowski et al., 1980; Nelson, 1980; Verdier et al., 1980; Van den Bark & Thomas, 1981; Muroaka & Kamata, 1983; Aitkenhead et al., 1985; Villemin & Sunwoo, 1987; Opheim & Gundmundsson, 1989; Walsh & Watterson, 1988; Gillespie, 1991; Marret & Allmendinger, 1991; Peacock, 1991; Gillespie et al., 1992; Gillespie et al., 1993; Dawers et al., 1993; Davison, 1994; Dawers & Anders, 1995; Cartwright et al., 1996; Jackson et al., 1996; Nicol et al., 1996; Schlische et al., 1996; Rowan, 1997; Fossen & Hesthammer, 1998	1.19	not given
Torabi et al., 2011	not given	MacMillan, 1975; Elliot, 1976; Muroaka & Kamata, 1983; Watterson, 1986; Villemin & Sunwoo, 1987; Walsh & Watterson, 1987; Krantz, 1988; Opheim & Gudmundsson, 1989; Peacock, 1991; Peacock & Sanderson, 1991; Gillespie et al., 1992; McGrath, 1992; Scholz & Cowie, 1992; Dawers et al., 1993; Gillespie et al., 1993; Cartwright et al., 1995; Villemin et al., 1995; Nicol et al., 1996; Schlische et al., 1996; Yielding et al., 1996; Gross et al., 1997; Wibberly et al., 1999; Kim et al., 2000; Walsh et al., 2002; Wilkins & Gross, 2002; Davis et al., 2005; Schultz et al., 2008	1	0.0001-1

258 **Table 1.** Table showing previously published global databases with the number of faults used and their sources, along with their values of *n* and *C* if given.

260 **3.3. Issues with previous D/L databases**

261 Several highly cited D/L and throw/L databases have been compiled in the past 35 years
262 (Walsh & Watterson, 1988; Cowie & Scholz, 1992a; Schlische et al., 1996; Bailey et al.,
263 2005; Torabi & Berg, 2011). Some of the data included in these contributions do not measure
264 true D or L, despite these data being reused in newer compilations. As a result, D/L scaling
265 laws could be affected. The way in which these data were presented, in non-digital format,
266 plotted tightly in log-log space, made the data unobtainable and non-replicable. We here
267 review these complications and suggest which data points could inaccurately skew D/L
268 scaling laws and should not be included in future databases.

269 Walsh & Watterson (1988) was, to the best of our knowledge, the first contribution that
270 compared the relationship between length (referred to as fault width) and displacement using
271 a global compilation of faults. 308 normal faults from the British Coalfields were compared
272 to a global dataset of 58 faults from 22 sources (Table 1). In that paper, the relationship
273 between fault length and displacement was described as $D=L^2/P$, where P (equivalent to c) is
274 a variable and related to rock properties, such as host rock shear modulus, (e.g., Cowie &
275 Scholz, 1992b; Bailey et al., 2005; Kim & Sanderson, 2005; Nicol et al., 2020). They use the
276 assumption that $n=2$ because all their data was bounded by a slope of 2, despite their data
277 having an overall regression line of $n=1.58$ (Walsh & Watterson, 1988). An average best-fit
278 equation was not given, so the average value of c is not known. Of the 22 sources included in
279 their dataset, nine had included data where D or L was not explicitly given, which could have
280 skewed their final D/L scaling law. For example, neither D and/or L were included in some of
281 the original sources used by Walsh and Watterson (1988) (Teas, 1929; Babenroth & Strahler,
282 1945; Brunstrom, 1963; Mayuga, 1970; Huntoon, 1974; Van den Bark & Thomas, 1980;
283 Aitkenhead et al., 1985). We note that Teas (1929) lists the measurement of the “closure
284 around the fault”, which was likely included as displacement, and Huntoon (1974) does not
285 explicitly state fault length and displacement. We therefore assume that Walsh & Watterson
286 (1988) may have established fault length and displacement from a schematic map of the study
287 area (see Figures 2, 3, 5, and 6 in Huntoon, 1974). In some papers, D and/or L were given as
288 a range rather than a single value (i.e., displacement ranges from 100-500 m; Shepherd &
289 Burns, 1978; Frost & Halliday, 1980), and Walsh & Watterson (1988) may have picked a
290 mid-point or maximum value of the range; this could possibly change the derived scaling
291 relationship, making the data appear over or under-displaced, depending on what value was

292 chosen. The data from Babenroth & Strahler (1945) and Huntoon (1974) were also originally
293 given as throw and was included in the Walsh and Watterson (1988) dataset as displacement,
294 which could make the faults look slightly over-displaced; throw data could be converted to
295 displacement if the fault dip is known or assumed, however this is not discussed in their
296 methodology. It is also entirely possible that correct fault length and displacement values
297 were given to Walsh & Watterson (1988), via personal correspondence with the authors,
298 however that was not included in the methodology or indicated by an in-text citation.

299 Cowie & Scholz (1992a) subsequently compared D/L relationships of ~210 faults compiled
300 from nine different sources, one of which overlaps with the sources used in Walsh &
301 Watterson (1988; Table 1). Their data suggest a linear D/L scaling relationship ($n=1$) (Cowie
302 & Scholz, 1992a), which would suggest an equation of $D=cL$. Average values of c are not
303 given. They note that large faults (defined as faults longer than 1 km) have a higher D/L ratio,
304 possibly since faults that cut through the brittle upper crust (usually faults with $L > 10$ km)
305 have a higher displacement (Cowie & Scholz, 1992a).

306 Of the nine sources used in Cowie & Scholz (1992a), four had potential errors in
307 measurement or included data from structures other than normal faults, which together could
308 have affected their D/L ratios. For example, thrusts (Elliot, 1976) and strike-slip faults
309 (MacMillan, 1975; Peacock, 1991) were included in Cowie & Scholz (1992a). Additionally,
310 neither D nor L data was presented in the data from Krantz (1988) (which contributed ~12 of
311 ~210 data points) so we cannot be sure where, geologically speaking, these values were
312 obtained from or how robust they are. Again, it is possible that the correct fault length and
313 displacement values were obtained via personal correspondence.

314 Schlische et al. (1996) compared 201 normal faults from the Dan River Basin, USA to a
315 global database of 346 faults from 11 sources, nine of which overlap with the earlier Walsh &
316 Watterson (1988) and Cowie & Scholz (1992a) compilations (Table 1). One of the key aims
317 of this paper was to compare the D/L relationship of small ($L < 1.25$ m) and larger faults.
318 They found that D/L did not vary as a function of fault size. Of the faults in their global
319 compilation, 174 were strike-slip faults from two different sources, and 172 were normal
320 faults from 11 different sources (Table 1). They note a broadly linear relationship between D
321 and L ($n=1$), with c values between 0.001 and 1; some of the variability in c could be due to
322 the inclusion of strike-slip faults in the dataset, which typically have a higher D/L ratio than
323 normal faults (Kim & Sanderson, 2005). The best fit curve through the compiled data is

324 arithmetically defined by $D=0.03L^{1.06}$, with the authors noting that there is no significant
325 change in the D/L scaling relation across many orders of magnitude.

326 Bailey et al. (2005) compared throw-length (rather than displacement-length) relationships of
327 their 7862 normal faults from the East Pennine Coalfield, UK to a global dataset of 1756
328 faults from 46 different sources, 22 of which overlap with Walsh & Watterson (1988), Cowie
329 & Scholz (1992a), or Schlische et al. (1996) (Table 1). Of the 46 sources used, 29 had
330 potential errors in measurement, included data that was not from normal faults, or were from
331 a source that was not publicly available; together, these issues could have affected the derived
332 D/L scaling law. For example, length and/or displacement/throw are not listed in the original
333 sources of several datasets (Beck, 1929; Teas, 1929; Babenroth & Strahler, 1945; Brunstrom,
334 1963; Woodland & Evans, 1964; Wood et al., 1969; Mayuga, 1970; Huntoon, 1974; Van den
335 Bark & Thomas, 1980; Aitkenhead et al., 1985; Gillespie et al., 1993). For example, Beck
336 (1929) only had displacement shown in a schematic cross-section, Krantz (1988) only
337 measured slip vector direction, Gillespie et al. (1993) measured fault spacing, and Gross et al.
338 (1997) measured maximum dip separation, yet all these values were included as throw.

339 Thrusts were included in the compilation (Fox, 1959; Elliott, 1976; Rowan, 1997), as well as
340 strike-slip faults (Freund, 1970; MacMillan, 1975; Peacock, 1991). Data from unpublished
341 (and still publicly inaccessible) theses were also included (MacMillan, 1975; Gillespie et al.,
342 1991), as were data from individual earthquakes (Jackson et al., 1996). Some faults had either
343 displacement or length listed as a range of values instead of a single measurement (see Figure
344 1) (Shepherd & Burns, 1978; Frost & Halliday, 1980). There were also some duplicate data,
345 where the same faults were studied in two separate papers and both were included; note that
346 this does not visually affect the data plot but can influence scaling relationship calculations
347 (Dawers et al., 1993; Dawers & Anders, 1995). Deformation bands were also included as
348 faults (Fossen & Hesthammer, 1998), with these structures having displacements up to two
349 orders-of-magnitude smaller than tectonic faults of the same length. Several sources
350 measured fault displacement in their original sources (Muroaka & Kamata, 1983; Ophem &
351 Gudmundsson, 1989; Walsh & Watterson, 1988; Marrett & Allmendinger, 1991; Dawers et
352 al., 1993; Nicol et al., 1996; Schliche et al., 1996), but were included in Bailey et al. (2005)
353 as throw. Despite these issues, the data compiled by Bailey et al. (2005) has been used in
354 several subsequent papers (Nicol et al., 2010, 2017; Reilly et al., 2017; Rotevatn et al., 2019;
355 Bramham et al., 2021).

356 To the best of our knowledge, the most recent compilation of D and L is by Torabi & Berg
357 (2011), who studied faults in siliciclastic rocks from 27 sources, 16 of which have overlap
358 with Walsh & Watterson (1988), Cowie & Scholz (1992a), Schlishe et al. (1996), or Bailey et
359 al. (2005) (Table 1). The total number of faults they include is unclear, as the data is very
360 tightly spaced in the presented scatterplot and the raw data are not available for analysis.
361 However, in the text they state these data are for normal faults from 22 sources, reverse faults
362 from four sources, and strike-slip faults from three sources (some sources had more than one
363 type of fault; Table 1). Torabi & Berg (2011) consider the potential causes of scatter in the
364 data, such as the underestimation of the frequency of small faults (truncation effect), and the
365 under-estimation of the frequency of long faults due to sample line limitations (censoring
366 effect). They found that small faults ($L < 1$ m) and large faults ($L > 1$ km) have a similar D/L
367 ratio, and that medium-sized faults ($L = 1$ -1000 m) tend to be comparatively under-displaced
368 (Torabi & Berg, 2011). They suggest this difference arises because medium-sized faults are
369 still growing by segment linkage, and that their D/L ratio will eventually match that of larger
370 faults as they mature (Torabi & Berg, 2011). They also found that strike-slip faults are over-
371 displaced compared to normal and reverse faults, and that cataclastic deformation bands are
372 under-displaced compared to faults (Torabi & Berg 2011). Length and/or displacement was
373 also not listed in the original sources of several datapoints (Krantz, 1988; Gillespie et al.,
374 1993. Vertical offset (i.e., throw) was measured in Villemin & Sunwoo (1987), which would
375 vary slightly from displacement.

376

377 **3.4. Methodology**

378 Our D/L database includes 4046 normal faults from 69 sources (Table 1), ranging in length
379 from 10 mm to 245 km, in age from the Carboniferous to presently active faults, and in
380 duration of activity from faults that were active for >100 Myr to those that have been active
381 for <1 Myr, and includes natural faults and those generated by physical and numerical models
382 (Table 2). Maximum length and maximum displacement are noted in our database, along
383 with fault host rock lithology, fault maturity, and tectonic history. We focused on these
384 parameters because they are known to affect fault growth (e.g., Cowie & Scholz, 1992a;
385 Torabi & Berg, 2011), and they provide a relatively easy and replicable way of characterizing
386 and comparing faults. All the data are provided in raw format and are publicly available, such
387 that the wider geologic community can easily access, analyze, and add to.

Source	Number of Faults	Data Type	Dominant Lithology	Reactivated	Size Range (length in m)	Active/inactive
Alghuraybi et al., 2021	18	3D seismic	Fine-grained clastic	No	4714-42,673 m	Inactive
Balsamo et al., 2016	23	Outcrop	Mixed carbonate & clastic		412-9290 m	Inactive
Blaekkan, 2016	43	Physical analogue			0.1-2 m	N/a
Bramham et al., 2021	768	Satellite imagery & topo data	Volcanic	Yes	16-2009 m	Active
Cartwright et al., 1995	91	Outcrop	Sedimentary & evaporites	No	280 m	Active
Crider & Pollard, 1998	2	Outcrop	Volcanic		1800-2200 m	Active
Dawers et al., 1993	15	Outcrop	Clastic w/ volcanic		20-2200 m	Active
Delokgos et al., 2017	16	Outcrop	Fine-grained carbonate		79-772 m	Active
Densmore et al., 2004	9	Outcrop	Clastic w/ volcanic		32,421-344,800 m	Active
Duffy et al., 2017	3	3D seismic	Mixed carbonate & clastic	Yes	4250-6738 m	Inactive
Ellis & Barnes, 2015	4	Outcrop	Carbonate		15,700-55,000 m	Varies
Ellis & Barnes, 2015	6	Outcrop	Clastic w/ volcanic		23,200-182,600 m	Active
Ellis & Barnes, 2015	1	Outcrop	Mixed carbonate & clastic		58,200 m	Active
Ellis & Barnes, 2015	3	Outcrop	Metamorphic, igneous & sedimentary		55,400-99,000 m	Varies
Finch & Gawthorpe, 2017	10	Numerical model			55,400-99,000 m	N/a
Gauthier & Lake, 1993	380	3D seismic	Clastic	Yes	71-1904 m	
Ghalayini et al., 2017	82	3D seismic	Fine-grained carbonate	No	5580-63,530 m	Inactive
Gillepsie et al., 1992	54	2D seismic	Fine-grained clastic		0.05-2.6 m	Inactive
Gross et al., 1997	121	Outcrop	Fine-grained clastic			Inactive
Gudmundsson, 2004	24	Outcrop	Volcanic	No	629-8982 m	Active
Hollinsworth et al., 2019	1	Outcrop & seismic	Metamorphic	Yes	15,440 m	Active
Hus et al., 2005	25	Physical analogue			0.14-0.4 m	N/a
Jackson & Rotevatn, 2013	4	3D seismic	Sedimentary & evaporites	Yes	5000-12,300 m	Active
Jackson et al., 2017	1	3D seismic	Sedimentary & evaporites		1950 m	Inactive
Karp et al., 2012	2	2D seismic	Metamorphic & clastic	Yes	23,873-27,140 m	Active
Khalil & McClay, 2017	3	3D seismic	Sedimentary & evaporites	Yes	12,000-23,000 m	Inactive
Kicono, 2005	1	2D Seismic	Metamorphic		6199 m	Active
Lamarche et al., 2005	3	2D Seismic	Clastic		225-436 m	Active
Lathrop et al., 2021	7	3D seismic	Mixed carbonate & clastic		8800-42,100 m	Inactive

Source	Number of Faults	Data Type	Dominant Lithology	Reactivated	Size Range (length in m)	Active/inactive
Marrett & Allmendinger, 1991	133	GPS & 2D seismic	Sedimentary & evaporites		1957-34,464 m	Inactive
McClymont et al., 2009	2	2D & 3D Seismic	Volcanic & clastic		30-47 m	Active
McGlue et al., 2006	2	2D Seismic	Metamorphic	Yes	17,014-51,000 m	Active
McLeod et al., 2000	32	3D seismic	Clastic		368-111,570 m	Inactive
Meyer et al., 2002	84	3D seismic	Mixed carbonate & clastic		690-8592 m	Varies
Morley et al., 2007	4	2D seismic	Clastic	Yes	6075-37,529 m	Inactive
Morley 2017	78	3D seismic	Mixed carbonate & clastic	Yes	3028-82,704 m	Inactive
Morley 2017	14	3D seismic	Fine-grained clastic	Yes	20,900-123,400 m	Inactive
Morley 2017	33	Outcrop	Sedimentary & evaporites	Yes	231-100,838 m	Inactive
Morley 2017	7	3D seismic	Clastic	Yes	30,845-91,792 m	Inactive
Muraoka & Kamata, 1983	14	Outcrop	Volcanic		0.6-2.5 m	Active
Nicol et al., 1996	112	3D seismic	Mixed carbonate & clastic	No	174-8926 m	Inactive
Nicol et al., 2005	1	2D seismic	Clastic	Yes	70,000 m	Active
Nicol et al., 2010	29	Aerial photography	Clastic w/ volcanic		2271-70,742 m	Active
Nicol et al., 2020	122	Outcrop & DEM	Carbonate		32-46,993 m	Active
Opheim & Gudmundsson, 1989	8	Outcrop	Volcanic	No	351-3383 m	Active
Pan et al., 2021	147	3D seismic	Mixed carbonate & clastic		307-18,182 m	Inactive
Peacock & Sanderson, 1991	6	Outcrop	Carbonate	No	7.2-226 m	Inactive
Poulimos, 2000	45	Outcrop	Mixed carbonate & clastic		1383-17,633 m	Active
Reeve et al., 2015	3	3D seismic	Clastic		1874-17,299 m	Inactive
Reilly et al., 2017	75	2D & 3D seismic	Clastic		1207-91,281 m	Inactive
Rippon, 1985	36	Outcrop	Clastic		200-4600 m	Inactive
Robert & Michetti, 2004	6	Outcrop	Carbonate		17,720-29,800 m	Active
Roche et al., 2017	5	Outcrop	Carbonate		0.26-3.7 m	Inactive
Schlishe et al., 1996	116	Outcrop	Fine-grained clastic		0.02-1.0 m	Inactive
Sieburg et al., 2020	432	Lidar	Volcanic		25-9707 m	Active
Solvia et al., 2005	36	Outcrop	Carbonate		0.3-50 m	Inactive
Solvia et al., 2006	50	Outcrop	Mixed carbonate & clastic		19-51 m	
Solvia et al., 2008	2	Outcrop	Carbonate		0.2-0.5 m	Inactive?

Source	Number of Faults	Data Type	Dominant Lithology	Reactivated	Size Range (length in m)	Active/inactive
Solvia et al., 2008	2	Outcrop	Mixed carbonate & clastic		0.8-1 m	Inactive
Solvia & Schultz, 2008	25	Outcrop			0.4-5 m	Active
Solvia & Schultz, 2008	34	2D seismic	Volcanic	No	66-53,700 m	Active
Shunshan et al., 2011	17	3D seismic	Sedimentary & evaporites	Yes	477-3298 m	Inactive
Torabi et al., 2019	21	3D seismic	Sedimentary & evaporites		238-23,255 m	Inactive
Tschopp 1967	1	2D seismic	Sedimentary & evaporites		45,000 m	Inactive
Tvedt et al., 2016	3	3D seismic	Sedimentary & evaporites	Yes	12,208-16,000 m	Inactive
Vétel et al., 2016	28	Satellite imagery & topo data	Volcanic	Yes	8772-29,467 m	Active
Villemin et al., 1995	26	Outcrop	Clastic		350-27,586 m	Inactive
Walsh & Watterson, 1988	32	Outcrop	Clastic		451-4985 m	Inactive
Walsh et al., 2002	22	Outcrop	Mixed carbonate & clastic	Yes	1200-18900 m	Active
Watterson, 1986	7				4799-53,645 m	
Wedmore et al., 2020	6	Outcrop	Metamorphic	Yes	13,000-85,000 m	Active
Whipp et al., 2014	176	3D seismic	Mixed carbonate & clastic		892-54,227 m	Inactive
Wibberly et al., 1999	28	Outcrop	Unlithified sand		0.17-10 m	Inactive
Wilkins & Gross, 2002	41	Outcrop	Clastic		0.9-490 m	Inactive
Willemse, 1997	7	Outcrop	Clastic w/ volcanic		47-151 m	Active
Williams et al., 2021	1	Outcrop	Metamorphic	Yes	130,000 m	Active
Worthington & Walsh, 2017	11	3D seismic	Fine-grained clastic	Yes	554-10,000 m	Inactive
Yielding et al., 1996	114	3D seismic	Fine-grained clastic		253-24,574 m	Inactive
Young et al., 2001	2	2D seismic	Clastic	Yes	11,00-12,000 m	Inactive
Zygouri et al., 2008	93	2D seismic & outcrop	Mixed carbonate & clastic		1764-15,147 m	Active

390

391

392

Table 2. Table showing all of the sources used in our global database, along with the number of faults from each source, type of data, host rock lithology, if the fault was reactivated or not, the range of fault sizes, and if the fault was active or inactive. Not all information was available for every source.

393 When displacement and length were not explicitly stated in the original sources, we used data
394 acquisition software (Quintessa Graph Grabber;
395 <https://www.quintessa.org/software/downloads-and-demos/graph-grabber-2.0.2>) to pick the
396 displacement and length from graphs. This yields a certain level of error, especially when
397 taking values from a graph in log-log space, because: (i) several overlapping data points may
398 only yield one datapoint; and (ii) there is some minor imprecision on where the extracted data
399 lie on the X (length) and Y (displacement) axis, which in a log-log plot could be moderately
400 significant (see Figure 1).

401 To be included, faults had to be normal (i.e., extensional) faults dominated by dip-slip
402 kinematics; reverse and strike-slip faults were not included. Fault length is defined as ‘the
403 longest horizontal or sub-horizontal dimension along the fault plane, perpendicular to slip
404 direction (Watterson, 1988; Kim & Sanderson, 2005). Fault displacement describes the
405 movement between two fault blocks, calculated by measuring an offset marker bed separated
406 by a fault (Walsh & Watterson, 1988; Xu et al., 2006). Displacement should be measured at
407 its maximum point on the fault. If throw was listed in the original source, it was converted to
408 displacement using the listed fault dip, or an average 55 degrees when fault dip was not
409 explicitly stated. All data are from geologic faults and not individual earthquakes. Faults have
410 been sorted and analyzed by size. We use length as a measure of fault size, defining three
411 classes: *small* (>1 m), *medium* (1 m-1 km), and *large* (>1 km) (see also Torabi & Berg,
412 2011).

413 Since host rock lithology might influence scaling laws, we sorted D/L data into the following
414 groupings: clastic (fine-grained sand and coarser), fine-grained clastic (siltstone and finer),
415 carbonate (specifically a carbonate ‘coarser’ than lime-mud), fine-grained carbonate (e.g.,
416 lime mud), mixed carbonate-clastic, evaporite-bearing sedimentary rocks, volcanic, volcanic
417 with clastic, and unlithified sand. Information on host rock lithology could not be found for
418 every fault, and it is only included in the database when explicitly listed by the author or
419 found in another source documenting the same basin. Faults often offset a variety of host rock
420 lithologies, especially for large faults, but they were categorized by the dominant lithology
421 (i.e., over c. 50%). ‘Carbonate’ host rocks are those with >50% carbonate material that is
422 coarser than lime-mud. Faults with host rocks classified as ‘clastic sedimentary’ have host
423 rocks whose lithologies are >50% clastic sedimentary rock, with sand-sized or coarser grains.
424 Faults with host rocks classified as sedimentary with evaporites have host rocks whose
425 lithologies are sedimentary rocks in areas with evaporites; not every fault is necessarily

426 physically linked to an evaporite detachment. Faults with host rocks classified as ‘fine-
427 grained clastic’ have host rocks whose lithologies are >50% clastic sedimentary rock with
428 silt-sized or smaller grain sizes. Faults in rocks classified as ‘fine-grained carbonate’ have
429 host rocks whose lithologies are >50% carbonate rock with fine-grained lithologies, such as
430 lime-muds. Faults in rocks classified as ‘mixed carbonate and clastic’ have host rocks whose
431 lithologies are roughly 50:50 clastic and carbonate. Faults with host rocks classified as
432 ‘unlithified’ were formed in unlithified sediment at the time of active faulting. Faults with
433 host rocks classified as ‘volcanic’ have volcanic host rocks. Faults in rocks classified as
434 ‘sedimentary with volcanics’ have both sedimentary and volcanic host rocks. Faults in
435 metamorphic host rocks were included in the overall dataset, however, there were not enough
436 of them to be statistically significant, so they are not separated in their own sub-group. To
437 compare the relationship between D/L to lithology and Young’s Modulus, we compiled a list
438 of known Young Modulus for different lithologies from published sources to find a range of
439 possible values and average value for each lithology; these data can be downloaded here
440 https://figshare.com/articles/dataset/Young_s_Modulus/17087342.

441 Faults were also classified based on tectonic history to assess how end-member tectonic
442 histories might affect their length and displacement. More specifically, we categorized them
443 as *reactivated* and *no pre-existing structures*; the former are from areas where faults clearly
444 reactivated structures that after a period of quiescence, became active again. These faults may
445 have formed in response to the reactivation of structures that previously experienced
446 extensional, compressive, strike-slip deformation, or a combination of these, before being
447 reactivated as normal faults. Faults categorized as having no pre-existing structures are from
448 areas thought to have not experienced significant earlier deformation. Information on tectonic
449 history is not always available, so not every fault is categorized this way.

450 Faults were classified as *active* and *inactive*; this allowed us to assess whether active faults
451 show different length and displacement relationships compared to inactive (i.e., dead) faults.
452 Faults categorised as active are from study areas where faults are currently active in
453 tectonically deforming regions, although every fault might not necessarily be active. Faults
454 categorised as inactive are from areas that are not tectonically active, i.e., inactive rifts now
455 buried and imaged in seismic reflection data or exposed in the field in exhumed basins. This
456 information is not available for every fault in the database, so not every fault is included in
457 this categorization. Care must be taken with these data because it is possible for an active
458 fault to be more to have been active for a long period of time and thus be over-displaced

459 compared to an inactive fault if the latter became inactive prematurely due to the removal of
460 the driving stress.

461 We stress that care must be taken when evaluating how these factors affect D/L scaling
462 relationships as it might be difficult or impossible to isolate the role of each. For example, if a
463 large fault is newly active, has a volcanic host rock, and formed due to reactivation of a pre-
464 existing structure, it may be difficult or impossible to determine which factors has the most
465 influence on its D/L ratio.

466 For each subcategory, we present the data in four ways: (i) in log-log space – even though
467 data can visually ‘hide’ in log-log space (Rotevatn et al., 2019), they allowed us to view all
468 data in one plot where all orders of magnitude can be seen together (ii) in non-log-log space,
469 with data shown all together in one graph spanning all orders of magnitude – this allowed us
470 to show overall D/L average trendlines, even though smaller faults cannot be visualised, (iii)
471 non-log-log space, grouped by order-of-magnitude so that all of the data can be seen more
472 clearly, (iv) and in a probability density plot. Probability density plots calculated the
473 probability density of D/L values in the each of the different aforementioned categories. We
474 used a kernel density estimation (KDE), which is a non-parametric method of estimating the
475 probability density of a function of a random value, in this case D/L. The height of each plot
476 (y-axis) corresponds to the probability density of the data at a given value of D/L (x-axis).
477 The peaks of the density plot are at the D/L values with the highest probability. A log-log
478 linear model (linear regression) was conducted to calculate a scaling law relationship of the
479 entire dataset, as well as each sub-category (i.e., fault size, tectonic history, fault maturity,
480 host rock lithology). Power law relationships were used because that is the standard in the
481 literature when relating fault displacement and length, and because it tended to fit the data
482 best. When describing faults throughout the paper, we refer to faults as over-displaced if
483 $D/L > 0.1$ and under-displaced if $D/L < 0.01$.

484

485 **3.5. Results**

486 In our database, faults are 0.01-344,800 m long (Figure 2) and have a power-law trendline of
487 $D_{max} = 0.03L^{0.92 \pm 0.01}$ (i.e., $n = 0.92 \pm 0.01$ and $c = 0.03$; Table 3). Our value of n is thus broadly
488 consistent with the estimate of Cowie & Scholz (1992a) and others ($n = 1$) for normal faults.
489 However, there is a large amount of scatter in our data, with displacements for a given fault
490 length ranging across 1.5-4 orders of magnitude (Figure 2). In this section we investigate how

491 D/L relationships are affected by fault size, maturity, tectonic history, and host rock
 492 lithology. We also look at examples of how D and L (and their related scaling relationship)
 493 change through time, assessing how this relates to the D/L global database, which is based on
 494 finite (i.e., present) fault geometry.

Category	Sub-category	Number	Number of Sources	Power-law Equation	R-squared
All faults	—	4035	65	$D_{max}=0.03L^{0.92\pm 0.01}$	0.85
Size	Small (0-10 m)	395		$D_{max}=0.04L^{0.97\pm 0.02}$	0.81
Size	Medium (10-10,000 m)	3246	48	$D_{max}=0.03L^{0.94\pm 0.01}$	0.63
Size	Large (10,000+ m)	394	35	$D_{max}=0.007L^{1.3\pm 0.01}$	0.24
Maturity	Active	1959	27	$D_{max}=0.02L^{0.92\pm 0.01}$	0.74
Maturity	Inactive	2059	38	$D_{max}=0.05L^{0.93\pm 0.01}$	0.92
Tectonic Setting	Reactivated	1620	8	$D_{max}=0.03L^{0.96\pm 0.01}$	0.74
Tectonic Setting	Not Reactivated	265	15	$D_{max}=0.04L^{0.87\pm 0.05}$	0.56
Lithology	Clastic Sedimentary	644	13	$D_{max}=0.11L^{0.84\pm 0.02}$	0.71
Lithology	Clastic w/ Evaporites	344	12	$D_{max}=0.02L^{1.04\pm 0.02}$	0.85
Lithology	Carbonates	181	7	$D_{max}=0.04L^{0.79\pm 0.03}$	0.97
Lithology	FG Carbonates	220	2	$D_{max}=0.06L^{0.93\pm 0.01}$	0.20
Lithology	FG Clastic	324	6	$D_{max}=0.03L^{0.94\pm 0.01}$	0.95
Lithology	Mixed Carbonate & Clastic	124	14	$D_{max}=0.04L^{0.92\pm 0.02}$	0.78
Lithology	Unlithified Sand	28	1	$D_{max}=0.01L^{0.72\pm 0.02}$	0.31
Lithology	Sedimentary w/ Volcanics	130	7	$D_{max}=0.007L^{1.0\pm 0.05}$	0.77
Lithology	Volcanics	1317	8	$D_{max}=0.04L^{0.82\pm 0.02}$	0.63

495

496 **Table 3.** Table listing of all the results for each of the studied categories, including number of faults, number of
 497 sources, power-law equation that can be used to estimate fault length or displacement, and the R-squared for
 498 that equation.

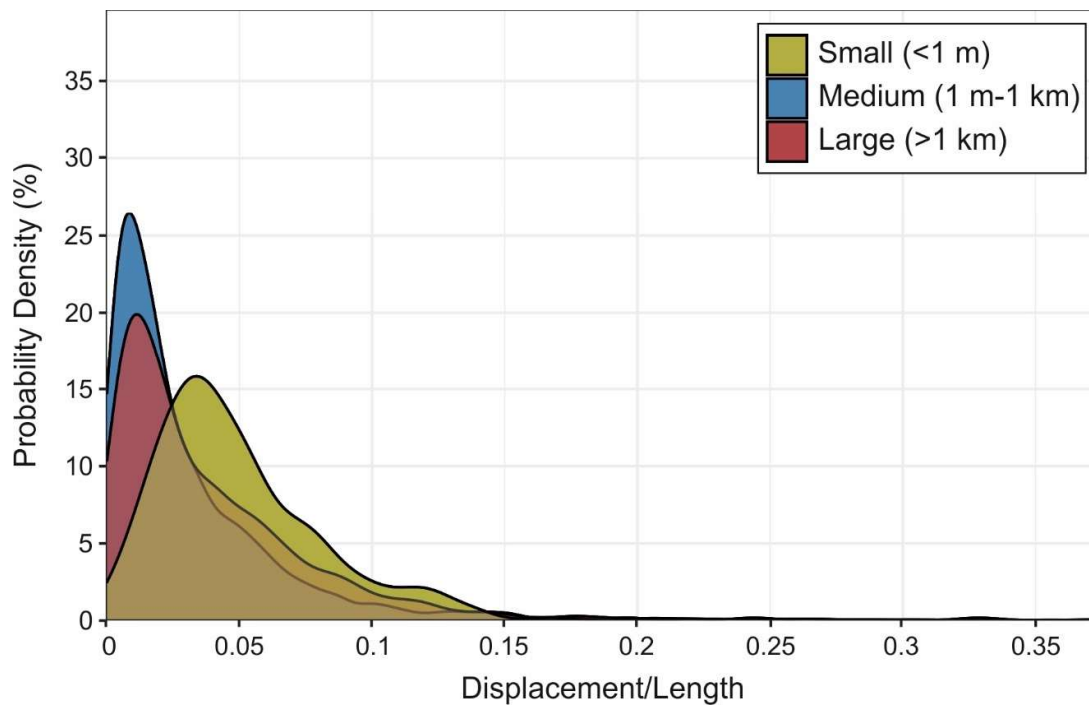
499

500 3.5.1. Size

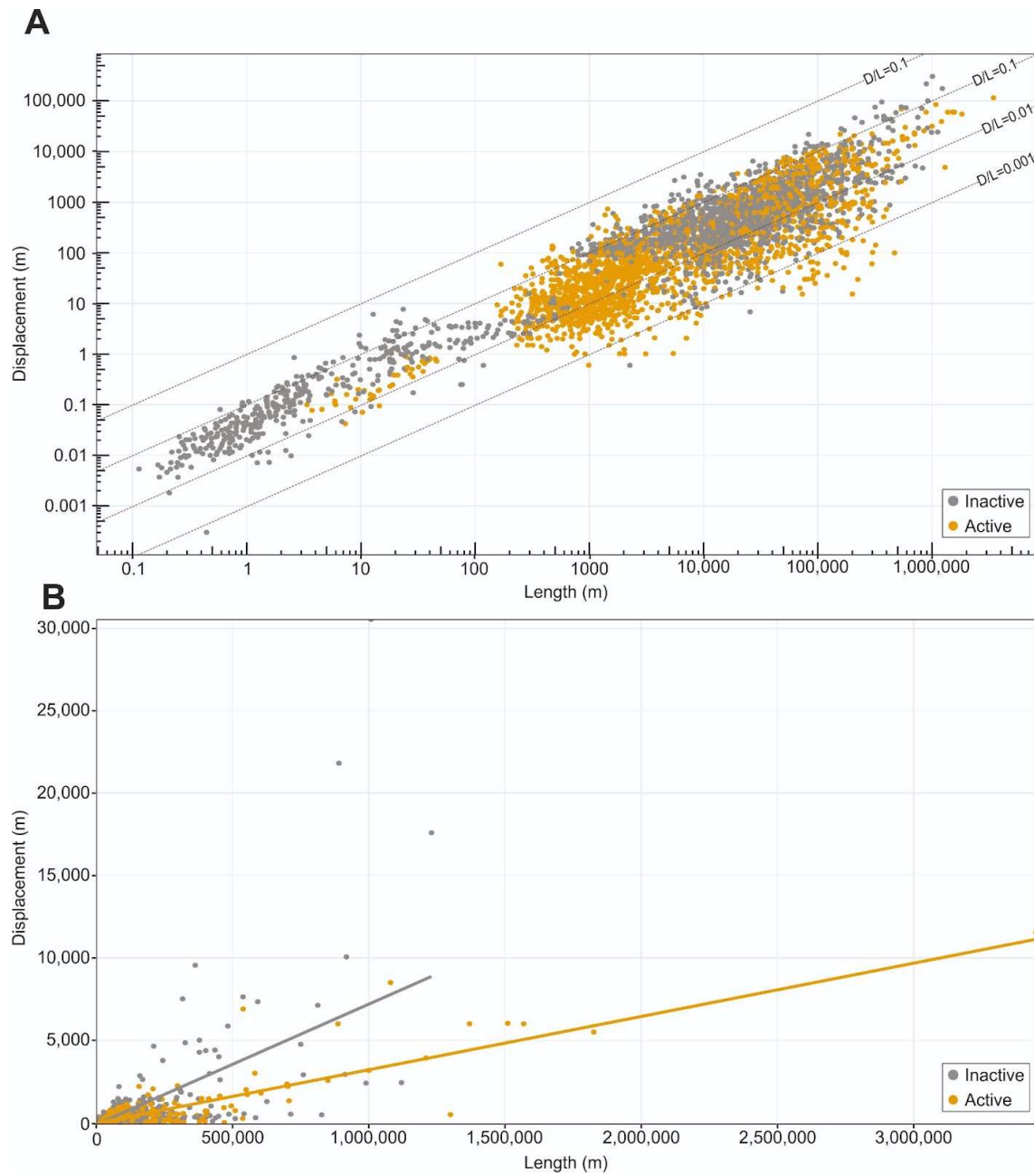
501 A total of 395 small faults were included from 11 different sources, 3246 medium faults were
 502 included from 48 sources, and 394 large faults were included from 35 sources (seen in Figure
 503 2). The dataset includes small faults from areas such as the High Atlas, Morocco and the Dan
 504 River Rift, USA, medium faults from areas such as the Pyrenees and Utah, USA, and large
 505 faults from areas such as the Levant Basin, offshore Lebanon, and the North Sea, offshore
 506 Norway. Our data show that small faults have a higher D/L ratio, with a power-law trendline
 507 indicating $D_{max}=0.04^{0.97\pm 0.02}$, $n=0.97\pm 0.02$ and $c=0.04$; Table 3). Medium and large faults
 508 have similar power-law trendlines of $D_{max}=0.03L^{0.94\pm 0.01}$ and $D_{max}=0.007L^{1.3\pm 0.01}$,
 509 respectively, $n=0.94\pm 0.01$ and $c=0.03$ for medium faults and $n=1.3\pm 0.11$ and $c=0.007$ for
 510 large faults (Table 3). The values of n of small are within the same confidence interval (Table
 511 3).

512 There is a significant amount of scatter in the relationship between D and L, especially for
513 larger faults (i.e., 3-4 orders of magnitude; Figure 2). For example, faults that are 10,000 m (\pm
514 200 m) long have displacements ranging from 4 m to 999 m, with a standard deviation of 303
515 m. In contrast, medium faults only vary by 1-2 orders of magnitude (Figure 2). For example,
516 faults that are 50 m (\pm 1 m) long have displacements ranging between 0.3 m and 7 m, with a
517 standard deviation of 1.6 m. Small faults have the least amount of scatter, with displacements
518 that vary by only 1-1.5 orders of magnitude (Figure 2). For example, faults that are 0.1 ± 0.05
519 m long have displacements between 0.002 m and 0.01 m, with a standard deviation of 0.003
520 m.

521 Medium and large faults plot similarly in a probability density plots (Figure 3); there is a
522 $\sim 27\%$ probability and $\sim 20\%$ probability, respectively, of a D/L value of ~ 0.02 , i.e., medium
523 to large faults in the dataset are most likely to have a displacement that is $\sim 2\%$ of fault length.
524 More small faults in the dataset were over-displaced compared to medium and large faults;
525 small faults have a $\sim 16\%$ probability of a D/L value of ~ 0.035 , i.e., small faults in this dataset
526 are most likely to have a displacement that is $\sim 3.5\%$ of fault length (Figure 3). The shape of
527 the distribution of small faults is relatively long-tailed, meaning that there are more small
528 faults with a higher D/L value than medium or large faults.



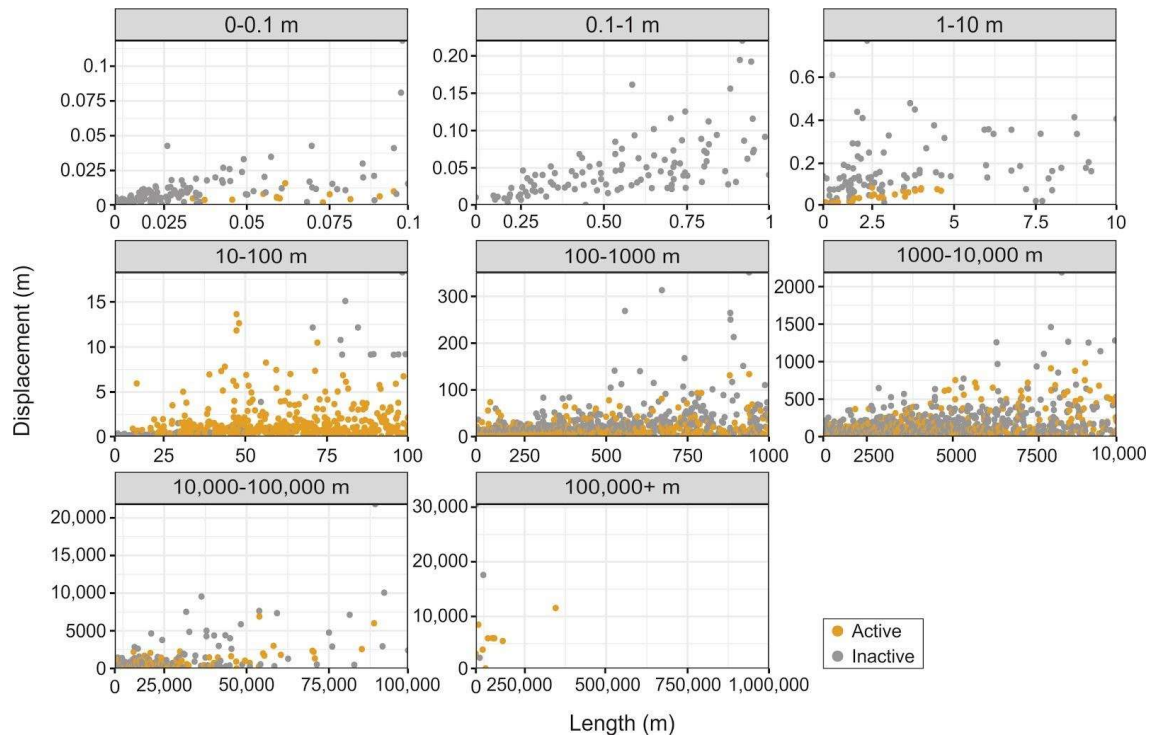
529 **Figure 3.** Density estimates of the D/L value of small, medium, and large faults in our dataset. Peaks in the
530 density plot are at the D/L values with the highest probability.
531



532

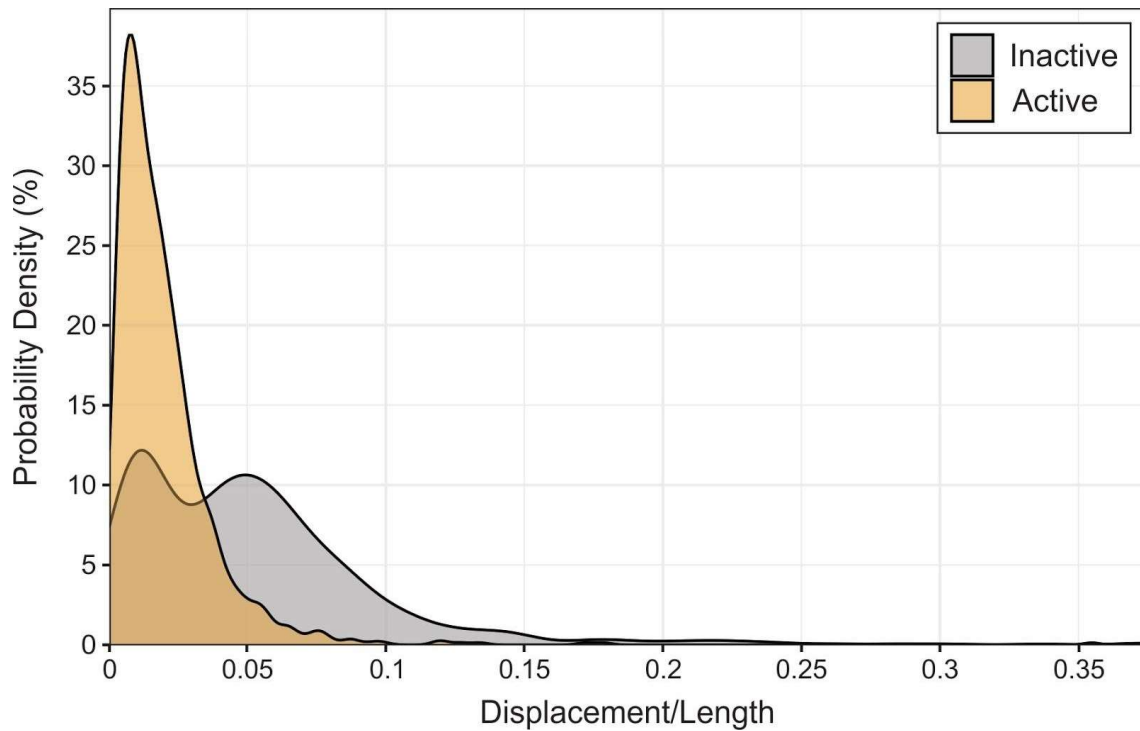
533 **Figure 4.** Plots showing fault length vs displacement for active and inactive normal faults in our database. A)

534 Data in log-log space. B) Data not in log-log.



535

536 **Figure 5.** Plots showing active and inactive normal fault D/L data, separated by order of magnitude.



537

538 **Figure 6.** Density estimates of the D/L value of active and inactive faults in our dataset. Peaks in the density
 539 plot are at the D/L values with the highest probability.

540

541

542 **3.5.2. Maturity**

543 1959 active faults from 27 sources were included, ranging in size from 0.3 m to 345 km in
544 length, with data from areas such as Crete, the Apennines, Italy, and the Turkana Rift, Kenya
545 (Figures 4-5). A total of 2059 inactive faults were included from 38 sources, ranging in size
546 from 0.01 m to 123.4 km in length, with data from areas such as the Exmouth Plateau,
547 offshore NW Australia, Horda Platform, offshore Norway, and the Levant Basin, offshore
548 Lebanon (Figures 4 and 5).

549 The active faults have a power-law trendline of $D_{max}=0.02^{0.92\pm 0.01}$, which requires
550 $n=0.92\pm 0.02$ and $c=0.02$, whereas inactive faults have a trendline of $D_{max}=0.05^{0.93\pm 0.01}$,
551 which requires $n=0.93\pm 0.01$ and $c=0.05$ (Table 3). The confidence values of n for inactive
552 and active faults overlap (Table 3). Inactive faults have a higher displacement/length ratio
553 than active faults (Figure 4b).

554 According to the probability density plot (Figure 6), there is a ~37% probability of active
555 faults having a D/L value of ~0.025, i.e., active faults are most likely to have a displacement
556 that is 2.5% of length. Inactive faults have two probability peaks; there is ~12% probability
557 of a D/L value of 0.025 and ~11% probability of a D/L value of 0.05, i.e., inactive faults are
558 most like to have a displacement that is ~2.5% or ~5% of length. The density plot of inactive
559 faults has a longer tail, which means that higher D/L values are more probable in inactive
560 faults than active faults.

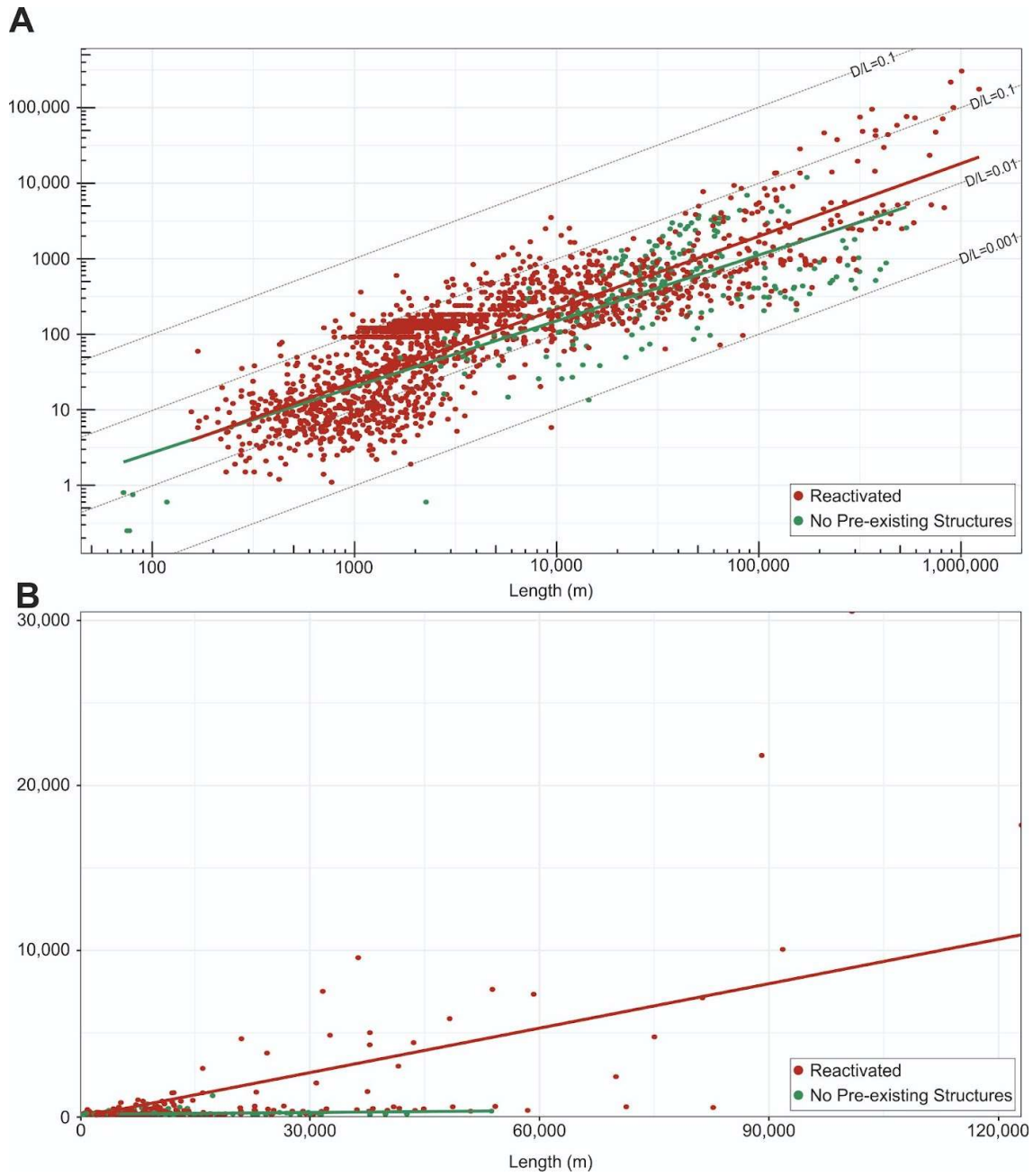
561

562 **3.5.3. Tectonic history**

563 1620 reactivated faults from eight sources were included, ranging in size from 17 m to 123
564 km in length, with data from areas such as the Porcupine Basin, offshore Ireland and the
565 North Malay Basin, Thailand (Figures 7 and 8). 265 faults with no pre-existing structures
566 were taken from 15 sources from areas such as Canyonlands, Utah, USA and the East Pacific
567 Rise (Figures 7 and 8). Faults range in size from 0.2 m to 54 km. The reactivated faults have
568 a power-law trendline of $D_{max}=0.03^{0.96\pm 0.01}$, $n=0.96\pm 0.1$ and $c=0.03$, and the non-
569 reactivated faults have a power-law trendline of $D_{max}=0.04^{0.87\pm 0.05}$, $n=0.87\pm 0.05$ and
570 $c=0.04$ (Table 3). Reactivated faults have a higher D/L ratio on average than faults not
571 forming in the presence of a pre-existing structure or structures (Figure 7b). This is unusual,
572 given several authors have suggested that reactivated faults tend to be under-displaced

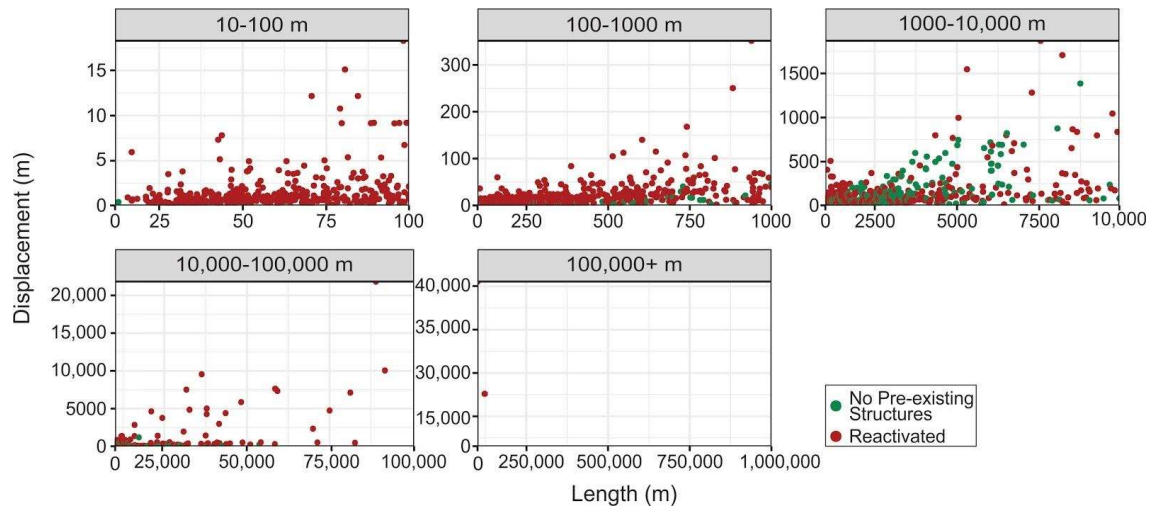
573 (Walsh et al., 2002; Vétel et al., 2005). We discuss the possible reasons for this in sub-section
574 5.3.

575 In probability density plots (Figure 9), reactivated faults and faults with no pre-existing
576 structures plot similarly; for reactivated faults and faults with no pre-existing structures, there
577 is a ~27% and ~24% probability, respectively, of a D/L value of ~0.025, i.e., both reactivated
578 faults and faults with no pre-existing structures in this dataset are most likely to have a
579 displacement that is ~2.5% of length. The distribution of reactivated faults has a slightly
580 longer tail, which means that there is a slightly higher probability of reactivated faults having
581 a higher D/L value.



582

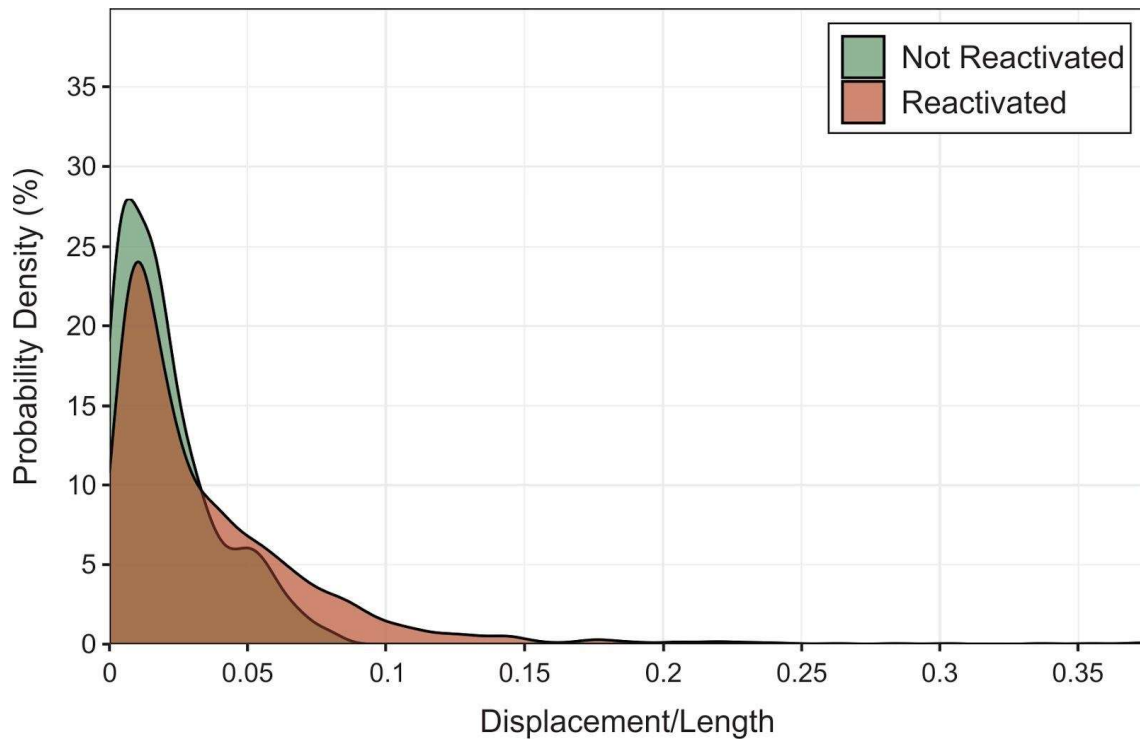
583 **Figure 7.** Plots showing fault length vs displacement for reactivated and non-reactivated normal faults in our
 584 database. A) Data in log-log space. B) Data not in log-log space.



585

586 **Figure 8.** Plots showing normal fault D/L data from reactivated faults and faults with no pre-existing structures,

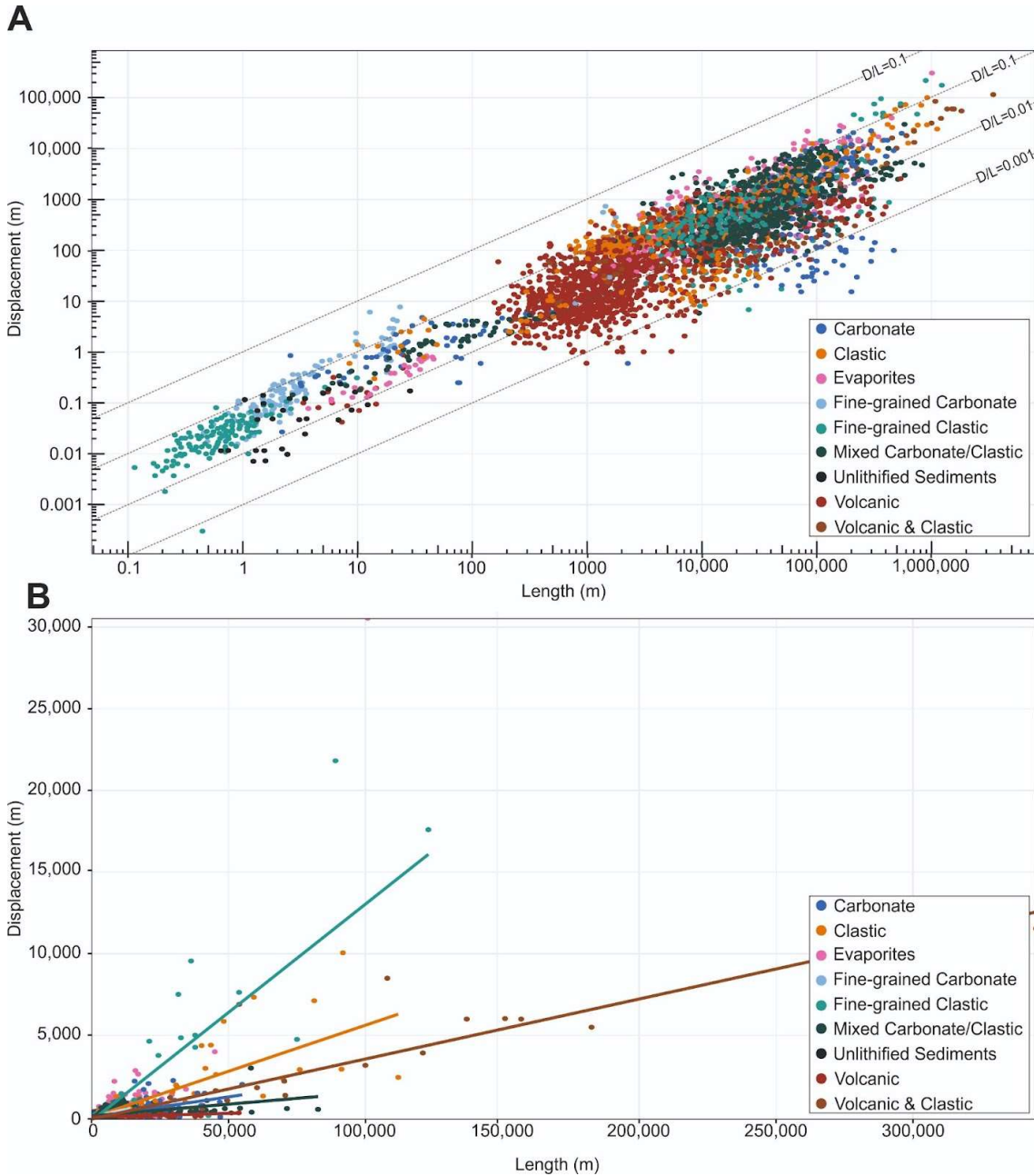
587 separated by order of magnitude



588

589 **Figure 9.** Density estimates of the D/L value of faults that have and have not been reactivated in our dataset.

590 Peaks in the density plot are at the D/L values with the highest probability.



591

592 **Figure 10.** Plots showing fault length vs displacement for normal faults with host rocks of different lithologies
 593 included in our dataset, including carbonate, clastic, evaporites, fine-grained carbonate, fine-grained clastic,
 594 mixed carbonate/clastic, unlithified sediments, volcanic, and volcanic/clastic. A) Data in log-log space. B)
 595 not in log-log space.

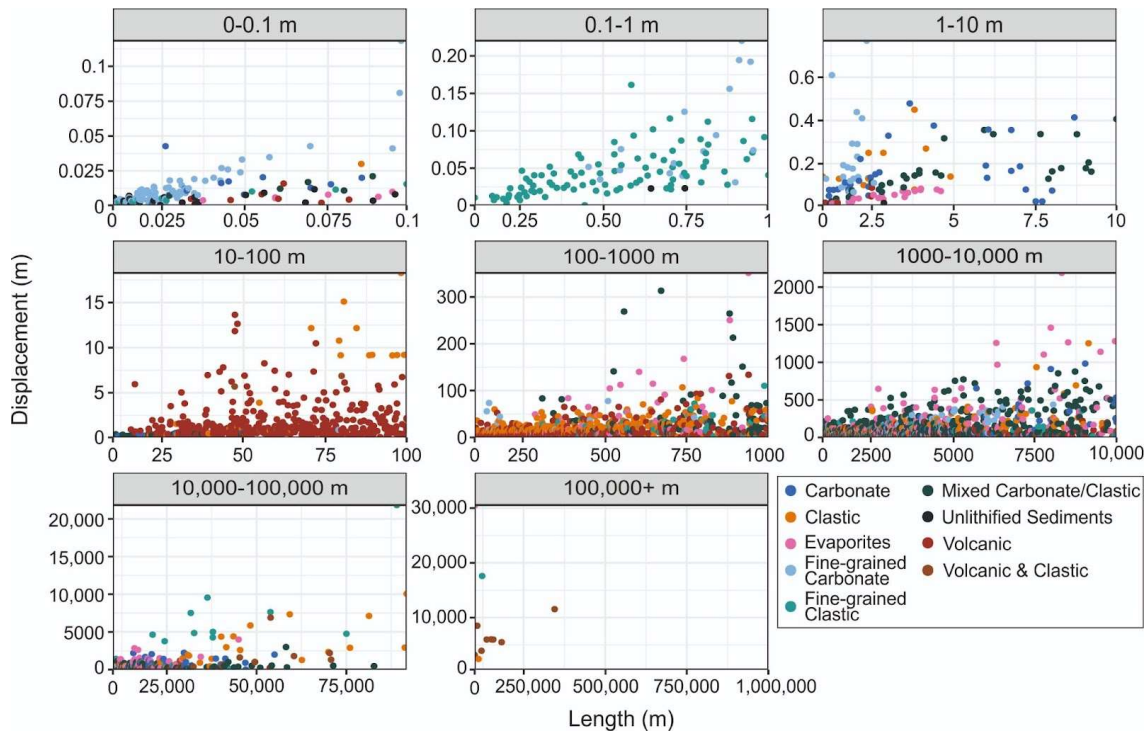
596

597 3.5.4. Lithology

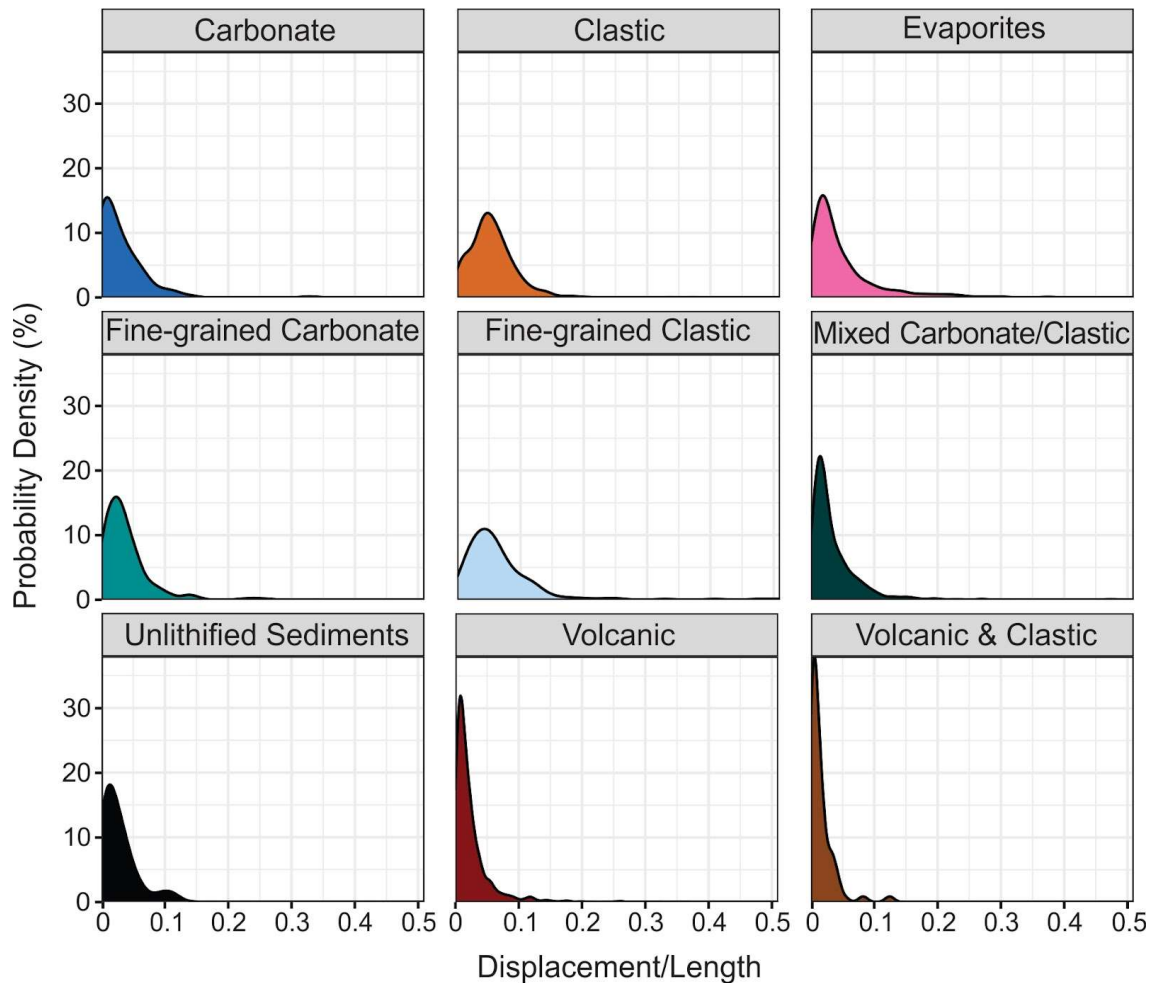
598 A power-law trendline was calculated for each lithology sub-category, with n values ranging
 599 from 0.007 to 1.1 and c values from 0.79 to 1 (Table 3). The confidence intervals for n of
 600 faults in fine-grained carbonate, fine-grained clastic, mixed carbonate/clastic, and
 601 sedimentary with volcanic rocks overlap and other host rocks do not (Table 3). Faults with

602 clastic sedimentary and fine-grained clastic sedimentary host rocks tend to have a higher D/L
 603 ratio (i.e., they are over-displaced) compared to the other lithologies (Figures 10 and 11).
 604 Faults with volcanic sedimentary and clastic with volcanic sedimentary host rocks tend to
 605 have a lower D/L ratio compared to the other lithologies (Figures 10 and 11).

606 According to density plots (Figure 12), clastic sedimentary rocks have the highest probability
 607 of high D/L values compared to the other lithologies, i.e., there is a ~13% probability of a
 608 fault in a clastic host rock having a D/L value of ~0.09, i.e., faults with clastic sedimentary
 609 host rocks in this dataset are most likely to have a displacement that is ~9% of the fault
 610 length. Faults with volcanic and clastic with volcanic host rocks have a higher probability of
 611 low D/L values than other lithologies; for volcanic and clastic with volcanic host rocks, there
 612 is a ~32% and ~35% probability respectively of a D/L value of ~0.01, i.e., faults with
 613 volcanic or volcanic/clastic host rocks are most likely to have a displacement that is ~1% of
 614 length.



615
 616 **Figure 11.** Plots showing normal fault D/L data for normal faults with host rocks of different lithologies
 617 included in our dataset, including carbonate, clastic, evaporites, fine-grained carbonate, fine-grained clastic,
 618 mixed carbonate/clastic, unlithified sediments, volcanic, and volcanic/clastic, separated by order of magnitude.



619

620 **Figure 12.** Density estimates of the D/L value of faults with host rocks of different lithologies included in our
 621 dataset, including carbonate, clastic, evaporites, fine-grained carbonate, fine-grained clastic, mixed
 622 carbonate/clastic, unlithified sediments, volcanic, and volcanic/clastic. Peaks in the density plot are at the D/L
 623 values with the highest probability.

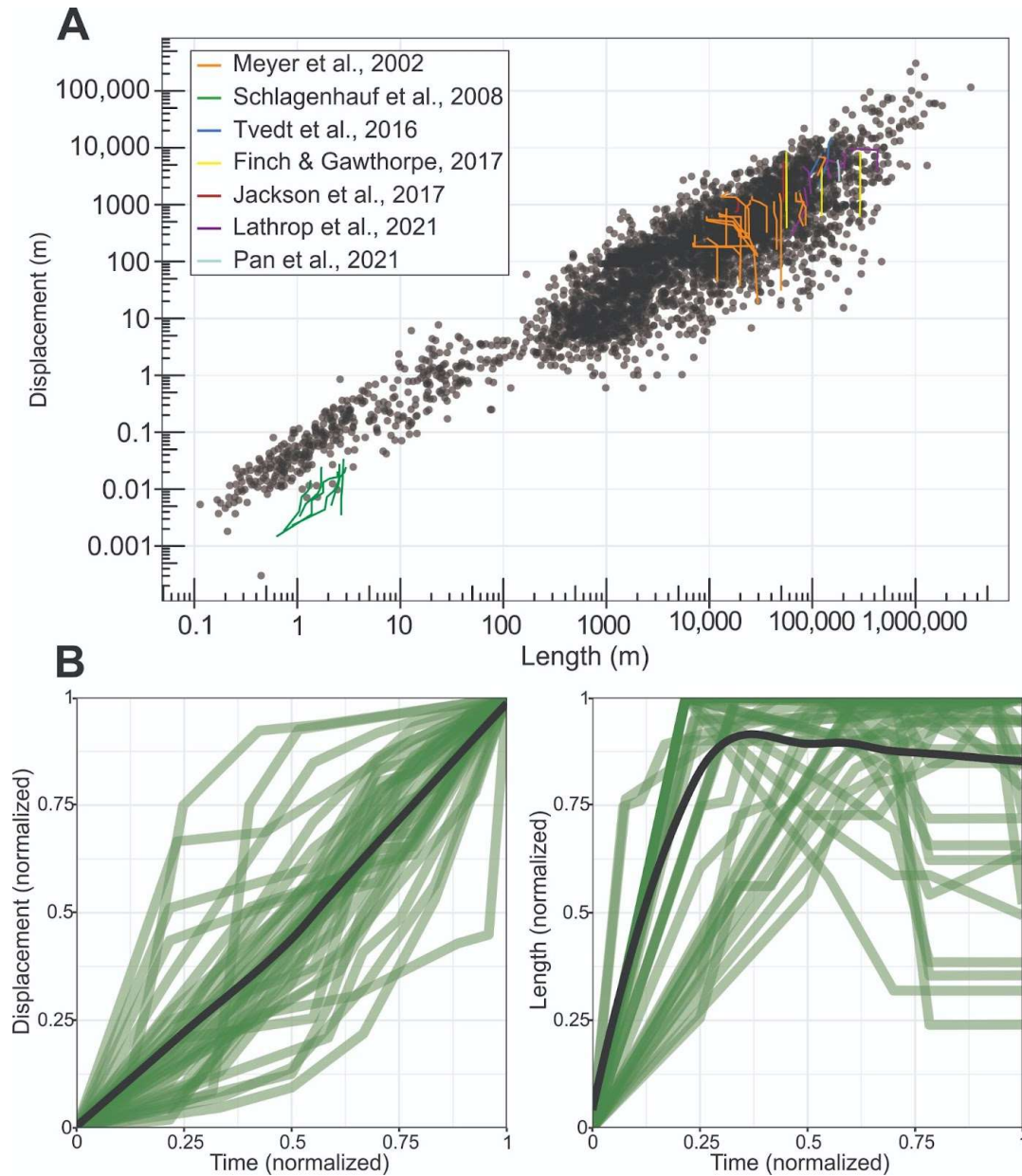
624

625 3.5.5. D/L through time

626 37 faults from six different sources were included in a dynamic D-L through time dataset
 627 (Figure 13). 24 natural faults imaged in 3D seismic reflection data were included, with these
 628 faults being 1.9-42 km long. Six faults generated in physical analogue models and three from
 629 numerical models were also included. The D/L trajectories of these faults are shown against
 630 the global D/L database (Figure 13a) and in normalised D vs. time and L vs. time plots
 631 (Figure 13b).

632 There is a wide range of displacement trajectories in the studied faults. For example, in the
 633 first 25% of the faults' lives, some faults had only accumulated only 6% of their (eventual)
 634 total displacement, whereas others had reached up to 75% of their final maximum
 635 displacement (Figure 13b). On average, faults accumulate displacement at a constant rate,

636 although on a fault-to-fault basis there is more variability (Figure 13b). 26 of the 37 (70%)
 637 faults attain >75% of their maximum length within the first 25% of their lives, and 35 of 37
 638 (95%) faults reach their lengths within the first half of their lives (Figure 13b). Faults then
 639 either maintain their maximum length or decrease in active trace length until they become
 640 inactive. On average, faults reach their maximum length within the first 30% of their lives
 641 and then decrease in length by 5-10%. 23 of the 37 (62%) faults experience late-stage lateral
 642 tip retreat, where their tips become inactive in the later stages of the faults' lives.



643

644 **Figure 13.** Figures showing fault growth through time (with data extracted from Meyer et al., 2002;
 645 Schlagenhauf et al., 2008; Tvedt et al., 2016; Finch & Gawthorpe, 2017; Jackson et al., 2017; Lathrop et al.,

646 2021; Pan et al., 2021). A) Global D/L dataset (black) for normal faults in log-log space with D/L through time
647 data in colour above it. B) Displacement and length through time, normalised in green, average values in black.

648

649 **3.6. Discussion**

650 We here summarise some key observations regarding the relationship between normal fault D
651 and L, and fault size, activity, tectonic history, and lithology, and then use specific, well-
652 constrained case studies to indicate how the various parameters control fault growth and
653 associated scaling relationships. We then discuss D/L changes through time, fault growth
654 models, and the processes that control the upper limits of the D/L scaling relationship.

655

656 **3.6.1. Size**

657 There is little consensus in the literature on how fault size affects the relationship between D
658 and L. Schlische et al. (1996) found no relationship between fault size and D/L ratio. In
659 contrast, Cowie & Scholz (1992a) found that very large faults (>1 km) were over-displaced
660 compared to smaller faults. Torabi & Berg (2011) showed that small faults (<1 m
661 displacement) and large faults (>1 km displacement) have a higher displacement/length ratio
662 than medium faults (between 1 m and 1 km), suggesting both small and large faults are over-
663 displaced. They explained that the low D/L ratio of medium-sized faults is likely due to faults
664 of this size being in the process of overlapping, interacting, and linking, i.e., they will
665 eventually become larger and accrue more displacement (Torabi & Berg, 2011). However,
666 the low D/L ratio of these faults could be due to sampling biases, i.e., there is a scarcity of
667 published medium-sized faults included in their database.

668 Our results show that large and medium-sized faults have similar displacement/length ratios,
669 but that small faults (<1 m) tend to be relatively over-displaced (Figure 3). Assuming a
670 constant-length growth model (e.g., Walsh et al., 2002; Jackson et al, 2017; Rotevatn et al.,
671 2019), faults reach their maximum length quickly and then accumulate displacement.
672 Medium and large faults are active for a longer period, and under a constant-length model
673 they are likely to have reached their maximum length and to be in some stage of displacement
674 accrual and thus be under-displaced. Under-displaced medium-to-large faults could either be
675 still active and in the displacement accrual stage or they could have become inactive before
676 they reached their maximum displacement potential (e.g., due to kinematic interactions
677 between faults, strain partitioning onto more optimally positioned faults). Small faults are
678 active for a shorter period, so faults can lengthen and accumulate a relatively high amount of

679 displacement and are less likely to become inactive before reaching their maximum possible
680 displacement.

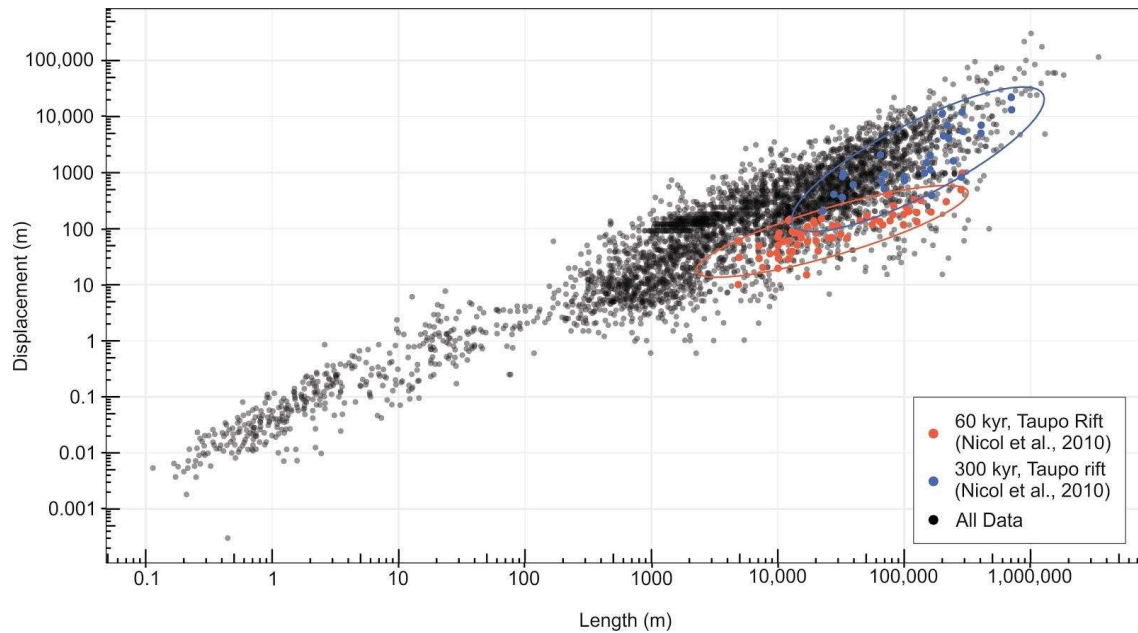
681 Duration of faulting may also explain scatter in the global D/L plot, i.e., the displacement on
682 large faults, which presumably have been active for longer than small faults, span up to four
683 orders of magnitude, whereas small faults only span 1-1.5 orders of magnitude (Figure 2).
684 Scatter for large faults represents faults that have become inactive prematurely, and the lack
685 of scatter for small faults may represent fault growth stages not detectable using, for example,
686 seismic reflection data (e.g., Jackson et al., 2017; Rotevatn et al., 2019).

687

688 **3.6.2. Maturity**

689 Fault length and displacement accumulation tend to be strongly partitioned in time (Figure
690 13b) (e.g., Walsh et al., 2002; Tvedt et al., 2016; Rotevatn et al., 2019). Thus, if the
691 maximum displacement had (in the case of an inactive fault) or has (in the case of a still-
692 active fault) been measured part-way through a fault's life rather than at the end, it would plot
693 as under-displaced, assuming a constant-length growth model. When estimating fault scaling,
694 it is important to keep in mind if the faults are active, and if so, how mature they are.
695 However, there is still a huge amount of scatter among both active and inactive faults;
696 inactive faults trend over-displaced compared to active faults (Figures 4 and 6), however the
697 scaling laws between inactive and active faults have n values with overlapping confidence
698 intervals (Table 3). Faults can become inactive at any point in their maturity, for example
699 dying pre-maturely with relatively low displacement, which could also add additional scatter.

700 We would expect that active faults tend to be younger and have been active for less time
701 compared to inactive faults; they are, therefore, could be comparatively under-displaced. This
702 aligns with our understanding of fault growth under a “constant length” or “hybrid growth”
703 model (Walsh et al., 2002, 2003; Nicol et al., 2005, 2017; Jackson & Rotevatn, 2013; Henstra
704 et al., 2015; Fossen & Rotevatn, 2016; Hemelsdaël & Ford, 2016; Tvedt et al., 2016; Childs
705 et al., 2017b). Under a constant-length or hybrid growth model, faults reach their maximum
706 length in the first 20-30% (or less) of their life. Active faults could be generally under-
707 displaced because they have reached their maximum length but are still accruing
708 displacement, however the relationship is not clear (Table 3).



709

710 **Figure 14.** Global D/L dataset (black) for normal faults in log-log space with faults of different maturities
 711 highlighted: 60 kyr faults from the Taupo Rift in orange and 300 kyr faults from the Taupo Rift in purple (from
 712 Nicol et al., 2010).

713 One example from the database of under-displaced, immature normal faults come from the
 714 Taupo Rift on the central North Island of New Zealand (Nicol et al., 2010; Figure 14). Rifting
 715 began 1-2 Ma, with the studied faults having been active for 60 kyr and 300 kyr. The area is
 716 tectonically active, and the faults accommodate 15 mm/yr of extension. The older faults,
 717 which have been active for 300 kyr, are 2.3 km to 70.7 km long and have displacements
 718 ranging between 20.7 m and 2198 m. D_{\max}/L is between 0.002- 0.06 (average 0.017) (Nicol et
 719 al., 2010; Figure 14). In contrast, the younger faults, which have been active for only 60 kyr,
 720 are 487 m to 28.7 km long, have displacements ranging between 1 m and 97.9 m, and a
 721 D_{\max}/L between 0.0009-0.01 (average 0.004) (Nicol et al., 2010; Figure 14). It is often
 722 difficult to deduce whether a fault is under-displaced due to fault maturity or lithology (see
 723 section 3); however, in the Taupo Rift case, given that these faults formed in the same host
 724 rock, it is likely these still-active faults are under-displaced solely due to fault maturity.

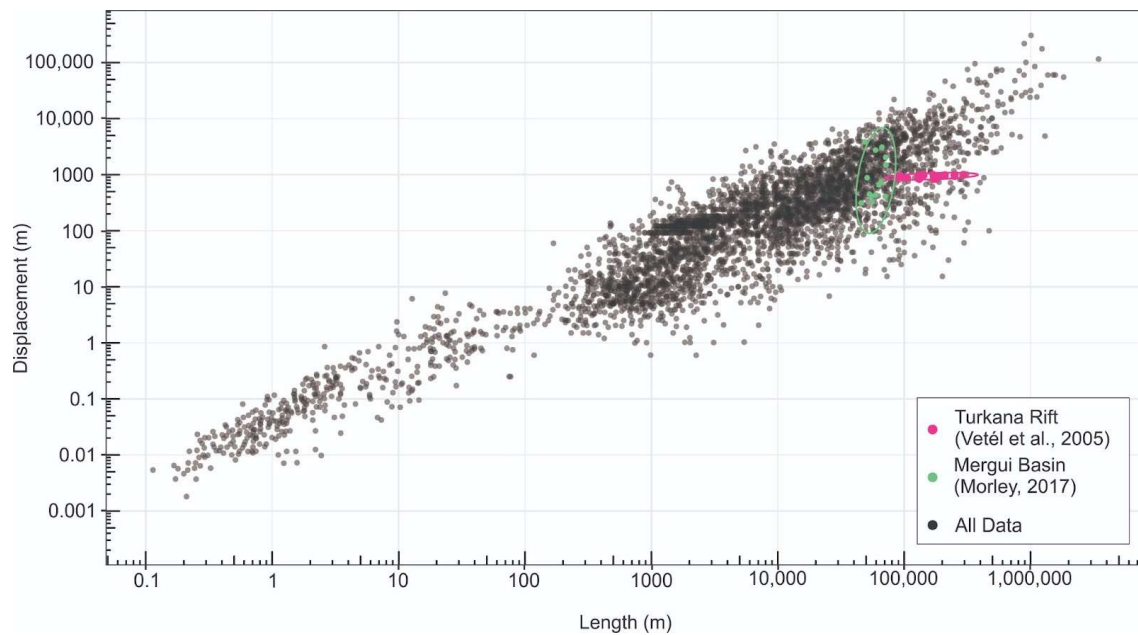
725 The Taupo Rift faults are under-displaced compared to a set of inactive faults of similar
726 length from the Exmouth Plateau, offshore NW Australia (Pan et al., 2021). Faults on the
727 Exmouth Plateau were active from the Early Jurassic-Early Cretaceous (85.5 kyr), are 307 m
728 to 181.2 km long, and have displacements ranging between 18.2 m and 857.6 m (Pan et al.,
729 2021). D_{max}/L is between 0.006-0.5 (average of 0.06). These faults grew in accordance with
730 and support the constant-length model, reaching their final length in less than 7.2 myr (8% of
731 their total lifespan) before accruing displacement (Pan et al., 2021).

732

733 **3.6.3. Tectonic history**

734 Faults that formed in response to the reactivation of a pre-existing structures tend to be
735 slightly under-displaced compared to faults in areas that have no reported pre-existing
736 faulting (Figure 7b and 9). Previous studies indicate reactivated faults tend to have a higher
737 displacement to length ratio because the maximum length of the fault is generally established
738 in the first phase of faulting (Vétel et al., 2005; Baudon & Cartwright, 2008). However, we
739 believe that role the reactivation of older structures and thus pre-extensional tectonic history
740 plays in controlling D/L ratios is strongly dependent on how long the fault has been active,
741 since newly formed faults will tend to be under-displaced, according to both the constant-
742 length and hybrid fault growth models (Rotevatn et al., 2019).

743 One example of reactivated normal faults is from the tectonically active Turkana Rift,
744 Northern Kenya (Vétel et al., 2005; Figure 15 in pink). Faults here range from 208 m-29.5
745 km long, have displacements ranging from 82.5 m to 101 m, and have been active for <3 Myr
746 (Vétel et al., 2005). Faults are thought to have reactivated Proterozoic basement faults, or
747 possibly utilised basement metamorphic foliation, and the area currently extends with a strain
748 rate of ~0.1 mm/yr (Vétel et al., 2005). Fault arrays were able to reach relatively long lengths
749 (~40 km) in a relatively short period of time, despite these relatively low strain rates, likely
750 due to them exploiting and activating pre-existing weaknesses (Vétel et al., 2005). The
751 average D/L ratio is 0.007, (displacement is 0.7% of length). These faults are thus under-
752 displaced, which is likely due to them having lengthened rapidly by exploiting intra-basement
753 weaknesses; these faults are thus likely still at the beginning of their displacement
754 accumulation stage.



755


756 **Figure 15.** Global D/L dataset (black) for normal faults in log-log space with reactivated faults highlighted:
 757 faults from the Turkana Rift in pink (from Vétel et al., 2005) and the Mergui Basin in green (from Morley,
 758 2017).

759

760 An example of more mature, but still-active reactivated faults come from the Mergui Basin,
 761 Thailand (Morley, 2017; Figure 15, in green), which unlike the Turkana Rift faults (Vétel et
 762 al., 2005) are relatively over-displaced. The area has a complicated tectonic history: the
 763 Mergui basin experienced Triassic-Early Jurassic and Early Cenozoic transtension, with the
 764 related strike-slip faults later reactivated as normal faults (Morley, 2017). These faults have
 765 been active since the Early Eocene to Late Miocene, are 20.9-123 km long, and have 458 m-
 766 21.8 km displacement (Morley, 2017). They are over-displaced, with a D/L average of 0.14
 767 (displacement is 14% of length), with D/L ratios as high as 0.26. These faults are over-
 768 displaced because they were able to establish their maximum length quickly by exploiting
 769 and reactivating pre-existing weaknesses inherited from previous faulting, and then
 770 accommodate strain by accruing displacement. These faults are still-active, but are very
 771 mature (i.e., they have been active since the Early Eocene); as a result, they have been able to
 772 attain high D/L ratios.

773 In summary, reactivated faults are, on average, over-displaced (Figures 7 and 9), and this
 774 should be considered when using D/L scaling laws to estimate faults length or displacement.
 775 However, we hypothesise that relatively young reactivated, still-active faults, such as the
 776 ones in the Turkana Rift (Vétel et al., 2005), could be under-displaced as they reached

777 maximum length quickly but are still accruing displacement. When assessing reactivated
 778 faults, it is important to consider how long the faults have been active.



Lithology	Young's Modulus (average)	Young's Modulus (range)	Average D/L ratio
Sedimentary w/ Evaporites	4-64 GPa (Evaporites)	23 GPa (Evaporites)	0.05
	0.04-67 GPa (Sedimentary rocks)	24 GPa (Sedimentary rocks)	
Fine-Grained Clastic Sedimentary	0.04-36 GPa	14 GPa	0.04
Clastic Sedimentary	6-67 GPa	25 GPa	0.06
Volcanic w/ Clastic Sedimentary	5-99 GPa (Volcanic)	49 GPa (Volcanic)	0.15
	6-67 GPa (Clastic Sedimentary)	25 GPa (Clastic Sedimentary)	
Carbonate	24-66 GPa	45 GPa	0.03
Mixed Clastic & Carbonate	24-66 GPa (Carbonate)	45 GPa (Carbonate)	0.04
	6-67 GPa (Clastic Sedimentary)	25 GPa (Clastic Sedimentary)	
Metamorphic	15.9-109 GPa	42 GPa	0.03
Volcanic	5-99 GPa	49 GPa	0.02

779

780 **Figure 16.** Figure showing how the Young's Modulus of different lithologies relates to D/L. The range of
 781 Young's Modulus, average Young's modulus, and average D/L for fault with host rocks of each lithology is
 782 shown. Generally, as Young's Modulus increases, D/L decreases. Our Young's Modulus data and sources can
 783 be accessed here: https://figshare.com/articles/dataset/Young_s_Modulus/17087342

784

785 3.6.4. Lithology

786 Host rock lithology can influence the relationship between fault length and displacement due
 787 to the stiffness of different lithologies, often described by host rock shear modulus (Walsh et
 788 al., 1988, 1989; Cowie & Scholz, 1992a; Wibberley et al., 1999). In previous studies an
 789 inverse relationship between host rock shear modulus and D/L has been reported; faults in
 790 host rocks with a high shear modulus (stiffer rocks, for example, a granite) are under-
 791 displaced compared faults with a high shear modulus (softer rocks, for example, a mudstone)
 792 (Walsh et al., 1988, 1989; Cowie & Scholz, 1992a; Wibberley et al., 1999; Gudmundsson,
 793 2004; Childs et al., 2017a).

794 The stiffness of rocks relates to their elastic properties, also expressed by the Young's
 795 Modulus and the Poisson ratio (Roche et al., 2013). Fault length and displacement have been
 796 related to rock stiffness in the following equation from crack models:

797

$$\frac{L}{D_{max}} = \frac{E}{2\Delta\tau(1 + \nu)}$$

798

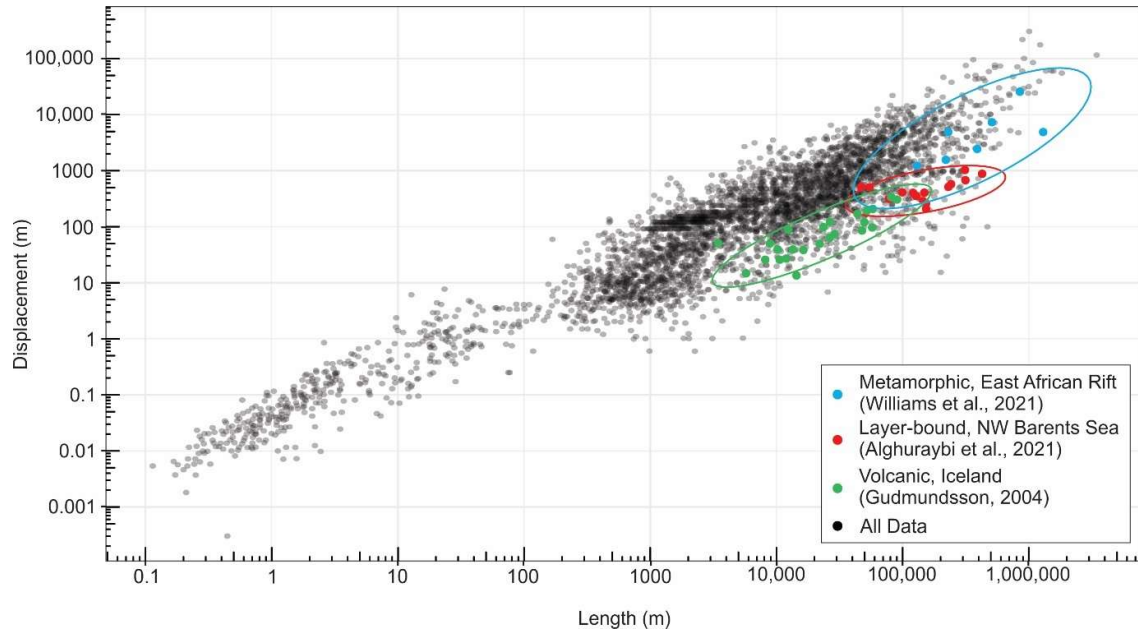
799

800 Where E is Young's Modulus, ν is Poisson's ratio, and $\Delta\tau$ is the shear stress driving the fault
801 (Roche et al., 2014). Poisson ratio can fall between 0.05 and 0.4, although values usually
802 range between 0.3 and 0.4 (Gereck, 2007). There is generally little variation in Poisson's ratio
803 between different lithologies, compared to Young's Modulus (Gudmundsson, 2004). Young's
804 Modulus has a high amount of variation, ranging between 0.05 GPa and 100 GPa (Roche et
805 al., 2013). Fault displacement is inversely proportional to the Young's modulus of the rock
806 (Wibberly et al., 1999, 2000a; Gudmundsson, 2004) which suggests that stiffer rocks, such as
807 volcanic and metamorphic rocks, are more likely to be under-displaced than pyroclastic or
808 sedimentary rocks. Factors such as increasing temperature, increasing porosity, and water
809 content can decrease Young's Modulus. Highly fractured rocks have a low Young's
810 Modulus; the breccia of a faults core has a low Young's Modulus, like that of a weak clay or
811 pyroclastic tuff (Gudmundsson, 2004).

812 The data compilation presented in this paper appears to reveal a relationship between the D/L
813 ratio of normal faults and host rock lithology, with faults with a low Young's Modulus
814 tending to have a higher D/L ratio (i.e., they are over-displaced) (Figure 16). Evaporite-
815 bearing sedimentary host rocks tend to be over-displaced compared to other lithologies,
816 which could be due to the softness of the rocks making tip propagation difficult. Both
817 evaporites and sedimentary rocks have a relatively low Young's Modulus, with sedimentary
818 rocks ranging between 0.04-67 GPa (24 GPa average; Figure 16) and evaporites ranging
819 between 4-64 GPa (23 Gpa average; Figure 16). Faults within either fine- and coarse-grained
820 clastic host rocks, are also relatively over-displaced, with Young's Modulus estimated
821 between 0.04-36 GPa (14 GPa average; Figure 16) for fine-grained clastic sedimentary rocks,
822 and 6-67 (25 Gpa average) for sandstones and conglomerates (Figure 16). Faults in
823 carbonates and mixed clastic/carbonates tend to lie in the middle of the various D/L
824 trendlines, with carbonates having an estimated Young's Modulus between 24-66 GPa (45
825 Gpa average; Figure 16). Faults within volcanic host rocks are significantly under-displaced
826 (Figure 10B), which is possibly in part due to the stiffness of volcanic rocks; volcanic rocks
827 have the highest estimated Young's Modulus, between 5-99 GPa (49 Gpa average; Figure
828 16).

829 One example of under-displaced faults in host rocks with a high Young's Modulus are in the
830 East African Rift (Figure 17; Williams et al., 2021). Here, normal faults are forming in a
831 metamorphic host rock. Fault ages are not well constrained, but they are estimated to be
832 roughly Pliocene in age and they are demonstrably still active (Scholz et al., 2020). Faults are

833 13 km to 130 km long and have displacements ranging from 122 m to 2.5 km. D_{max}/L is
 834 very low, between 0.003-0.03 (average of 0.01), indicating the faults are relatively under-
 835 displaced (Williams et al., 2021). It should be noted that these faults are active, which as
 836 discussed in section 2 could result in them being under-displaced. Additionally, some of the
 837 faults in the East African Rift have reacted foliation, making it ambiguous as to whether these
 838 faults being under-displaced are related to Young's Modulus, fault maturity, reactivation, or a
 839 combination.



840
 841 **Figure 17.** Global D/L dataset (black) for normal faults in log-log space with faults from different host rocks
 842 highlighted: metamorphic host rocks from the East African Rift (from Williams et al., 2021), layer-bound faults
 843 from the NW Barents Sea in red (from Alghuraybi et al., 2021), and volcanic host rocks from Iceland (from
 844 Gudmundsson, 2004).

845
 846 Another example of under-displaced normal faults within stiff host rocks come from an
 847 active rift zone in Iceland (Figure 17; Gudmundsson, 2004). The faults here are Holocene
 848 (<10,000 years old) and cut through basaltic pahoehoe lava flows with an estimated Young's
 849 Modulus of 30-60 GPa, and possibly as high as 100 GPa. Faults range from 345 m to 9 km
 850 long and have displacements ranging from 1.3 m to 33 m. D_{max}/L is between 0.0009-0.01
 851 (average of 0.004), meaning the faults are under-displaced (Gudmundsson, 2004). We expect
 852 the stiff host rock lithology has contributed to these faults being under-displaced; however,
 853 these are active faults, so according to a constant-length fault growth model, they have
 854 possibly reached their maximum length, but not yet their maximum displacement.

855 Differences in mechanical stratigraphy between lithological units can create vertical barriers
856 that inhibit fault growth, which can cause faults to be under-displaced (Peacock & Sanderson,
857 1992; Wilkins & Gross, 2002; Welch et al., 2009; Roche et al., 2014). There is a relationship
858 between rock stiffness and fault displacement gradient (i.e., the displacement variation per
859 unit length across a fault), with these gradients tending to be higher in rock units with lower
860 Young's Modulus (Roche et al., 2014). Mechanical stratigraphy can restrict faults from
861 propagating vertically, causing faults to have a high aspect ratio (fault height/length; height is
862 the fault dimension along dip) (Nicol et al., 1996; Schultz & Fossen, 2002; Soliva et al.,
863 2006; Roche et al., 2013; Alghuraybi et al., 2021). In a numerical modelling analogue study
864 by Roche et al. (2013), aspect ratios for faults in homogeneous rock properties not bounded
865 by mechanical stratigraphy are typically >2 , whereas aspect ratios of faults in limestone-clay
866 sequences are, on average, 13, and even as high as 50 (Roche et al., 2013). However, no
867 aspect ratios >20 have been reported in natural studies (Torabi et al., 2019). If faults have a
868 high aspect (height-length) ratio, it stands that they would likely also have a high
869 displacement-length ratio. However, this is likely only applicable to relatively small faults, or
870 possibly large faults cutting through thick layers (e.g., a fault with 1 m of displacement
871 offsetting a 20 cm-thick mudstone package, vs. a 1 km displacement fault offsetting a 100 m-
872 thick mudstone package).

873 One example of under-displaced faults with high aspect ratios included in our database are
874 layer-bound, thin-skinned normal faults from the NW Barents Sea (Figure 17; Alghuraybi et
875 al., 2021). The faults in this study were only active in the Late Jurassic and they occur in a
876 fine-grained clastic host rock. Faults are 4.7 km to 42.7 km long, have displacements ranging
877 from 21 m to 103 m, and their D_{\max}/L is between 0.001-0.009 (average of 0.003). They have
878 aspect ratios as high as 19, compatible with aspect ratios found in the numerical models of
879 Roche et al. (2013). The faults from the NW Barents Sea are interpreted to have reached their
880 final length quickly (i.e., they grew in accordance with the constant-length model) and were
881 not able to reach their likely maximum displacement, likely due to the mechanical layering.

882 In summary, host rock lithology influences D/L ratios; softer rocks (such as sedimentary
883 rocks) tend to be over-displaced, and stiffer rocks (such as volcanic rocks) tend to be under-
884 displaced, which agrees with the initial hypothesis from previous literature (Wibberly et al.,
885 1999, 2000a; Gudmundsson, 2004). Mechanical stratigraphy also causes rocks to be
886 vertically restricted and causes them to be under-displaced.

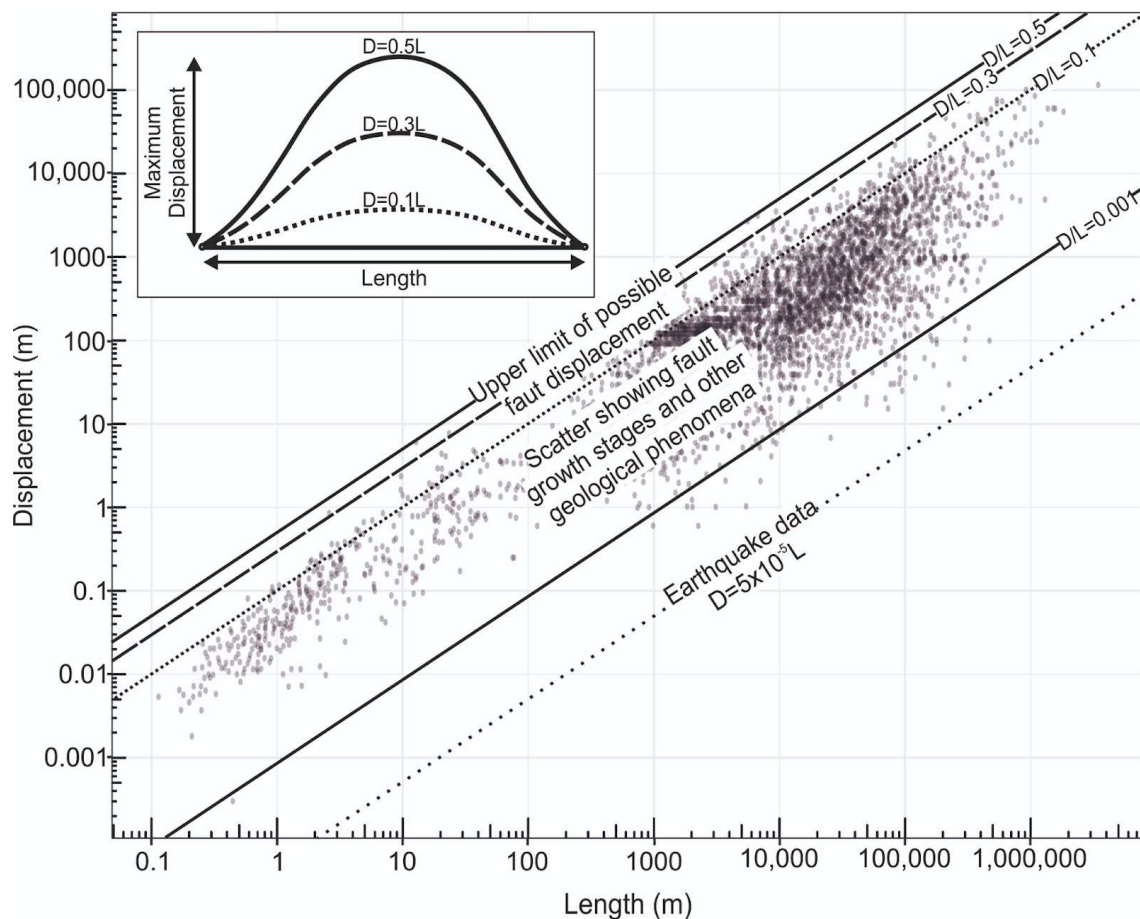
887

888 **3.6.5. How useful are D/L scaling laws?**

889 Our overall scaling relationship between normal fault length and maximum displacement for
890 all data in our revised database is $D=0.03L^{0.92\pm0.01}$. This agrees with previous literature that
891 estimated $n=1$ (Cowie & Scholz, 1992a; Dawers et al., 1993; Scholz et al., 1993; Clark &
892 Cox, 1996; Schlische et al., 1996; Kim & Sanderson, 2005; Xu et al., 2006). Our database has
893 thousands of faults that span eight orders of magnitude in terms of fault length, thus we
894 believe that we can confidently say that, overall, $n=1$, and that our equation could be used to
895 reliably estimate D or L within 1-2 orders of magnitude in most cases.

896 There is so much variability in our plots ($r^2=0.85$) when all D/L data is considered that it
897 could be questioned whether a single global scaling law should be used at all. Even after
898 conducting a detailed quality check of the data and removing data for which we believe there
899 are errors/inconsistencies, there is still significant variation in the D/L scaling relationship for
900 normal faults. As we discuss above, we suggest that some of these differences may be related
901 to properties such as lithology, fault maturity and reactivation. The scaling relationships for
902 data within each of these categories are different, however in some cases overlap within the
903 confidence intervals. This may be related to the fact that feedbacks between the properties
904 considered in this study likely exist and more analysis is needed to establish which are the
905 key properties which most control D/L. Despite this, we believe that there *is* value in being
906 able to estimate D from L, and that more specialised scaling relationships like those provided
907 here considering fault size, lithology, tectonic history, and fault maturity are thus warranted.
908 For example, using our global scaling law ($D_{max}=0.03L^{0.92}$), we would estimate that a 3 km
909 long normal fault within a sandstone host rock in a tectonically active area would have a
910 displacement of c. 47 m. In contrast, if we use the ‘clastic sedimentary’ D/L equation
911 ($D_{max}=0.11L^{0.84}$), we would estimate a displacement of c. 277 m; by using the ‘inactive’ D/L
912 equation ($D_{max}=0.05L^{0.93}$) we would estimate a displacement of c. 126 m. Both values are
913 likely more accurate than the global estimate, which may have implications for situations
914 which require estimating fault displacement or length, such as understanding fault sealing,
915 possible CO₂ leakage in a potential CCS locality, how large an earthquake might be. For the
916 most accurate estimates, we would suggest either 1) calculating an average of the applicable
917 equations, in this example, an average between the value for a ‘clastic sedimentary’ and
918 ‘inactive’, or to have an even more accurate estimation, 2) use our database to combine faults
919 with similar factors to make a bespoke equation for that area.

920 The relationship between fault D and L is also dynamic, changing throughout a fault's life. It
 921 is important to practice caution when working with D/L ratios. As shown in Figure 13, the
 922 relationship between D and L evolves through time, thus using static data to infer a dynamic
 923 relationship can be problematic. Plotting data only in log-log space can hide variability and
 924 statistical spread, as shown by Rotevatn et al. (2019). For example, different stages of fault
 925 growth will likely be masked in a large log-log plot, as the fault lies within the global scatter
 926 at every stage of fault growth. This shows that fault growth cannot be inferred from global
 927 D/L plots, and that plotting D and L *through* time (Figure 13) is important to understanding
 928 fault growth.



929
 930 **Figure 18.** Global D/L dataset for normal faults with our suggested upper limit of D/L ($D/L=0.1$). The average
 931 D/L value of a single earthquake is also shown (Wells & Coppersmith, 1994).

932
 933 **3.6.6. Upper bounds of displacement**

934 In contrast to the lower limits of the D/L scaling dataset, which shows significant scatter
 935 likely reflecting the process of fault growth, there appears to be an upper limit of maximum
 936 displacement (Figure 18). The absolute upper bound is the upper limit of $D_{max}/L=0.5$ (i.e., at

937 max, faults displacement can be $\frac{1}{2}$ of length), however very few faults have a D/L value that
938 high, i.e., 99.7% of the data falls below $D/L = 0.3$, and 94% of the data falls below $D/L = 0.1$.
939 We argue that the D/L upper-limit seen in our global dataset may be related to an overarching
940 rule of fault mechanics in which faults cannot accommodate a certain amount of
941 displacement without additional propagation or linkage with another fault. The wall-rock that
942 borders the fault tips can accommodate a finite amount of shear stress, and beyond that the
943 rock will fail, resulting in additional fault tip propagation (Freeman et al., 2010). Upper D/L
944 limits could also be due to isostatic restoring forces due to the topography generated in the
945 hanging wall and footwall blocks of the fault (Cowie & Scholz, 1992a).

946 **3.7. Conclusions**

947 We here present a new normal fault database that presents fault length and displacement
948 along with host rock lithology, fault maturity, and tectonic history that will now be available
949 to the public. In our interrogation of the new global normal fault database of 4046 faults, we
950 found that 1) for the complete dataset $n=0.92$ in terms of the standard equation $D_{max}=cL^n$,
951 but there is a lot of scatter in D/L in the global dataset when faults of all lithologies,
952 maturities, and tectonic histories are grouped together, 2) small faults (> 1 m) tend to be over-
953 displaced, 3) stiffer rocks tend to be under-displaced, and softer rocks tend to be over-
954 displaced, 4) active faults tend to be over-displaced compared to inactive faults, and 5)
955 reactivated faults are over-displaced compared to faults in previously undeformed settings,
956 unless the reactivated faults are still active. We also collected normal fault D/L through time
957 data and found that faults grow via a constant length-to-hybrid fault growth model. Since D/L
958 ratios are changing throughout a fault's life, it is important to express caution when looking at
959 static D/L data.

960 **Acknowledgements**

961 We thank Imperial College for providing Bailey Lathrop with the President's Scholarship to
962 fund their PhD research. Whilst compiling this data, we received an outpouring of support
963 from Twitter and the Geotectonics mailing list, and we are grateful to each person that
964 reached out to share data with us. We thank Alex Lipp and Sinead Lyster for their advice
965 during the data analysis portion of this research. We thank Alex Whittaker and Clare Bond
966 for their feedback provided during Bailey Lathrop's PhD viva. We also thank the Imperial
967 College Basins Research Group (BRG) for their feedback and help throughout this research.

968 **Data availability statement**

969 The databases compiled for this paper are available open-access via Figshare
970 (<https://doi.org/10.6084/m9.figshare.17087273>). All sources used in these databases are cited
971 within. Young's Modulus values for the different lithologies analysed were also compiled
972 and can be accessed via Figshare (<https://doi.org/10.6084/m9.figshare.17087342.v1>).

973 Sources

- 974 Ackermann, R. V., Schlische, R. W., & Withjack, M. O. (2001). The geometric and statistical
975 evolution of normal fault systems: An experimental study of the effects of mechanical
976 layer thickness on scaling laws. *Journal of Structural Geology*, 23(11), 1803–1819.
977 [https://doi.org/10.1016/S0191-8141\(01\)00028-1](https://doi.org/10.1016/S0191-8141(01)00028-1)
- 978 Acocella, V., Gudmundsson, A., & Funicello, R. (2000). Interaction and linkage of extension
979 fractures and normal faults: examples from the rift zone of Iceland. *Journal of Structural*
980 *Geology*, 22, 1–14. [https://doi.org/10.1016/S0191-8141\(00\)00031-6](https://doi.org/10.1016/S0191-8141(00)00031-6)
- 981 Aitkenhead, N. (1985). Geology of the country around Buxton, Leek and Bakewell. Mere.
982 geol. Surv. Gt. Br., sheet 111.
- 983 Alghuraybi, A., Bell, R. E., & Jackson, C. A. (2021). The geometric and temporal evolution
984 of fault-related folds constrains normal fault growth patterns, Barents Sea, offshore
985 Norway. *Basin Research*, July, 1–22. <https://doi.org/10.1111/bre.12633>
- 986 Alnuaim, A., Hamid, W., & Alshenawy, A. (2019). Unconfined Compressive Strength and
987 Young's Modulus of Riyadh Limestone. *Electronic Journal of Geotechnical*
988 *Engineering*, 24(3), 707–717.
- 989 Babenroth, D. L. & Strahler, A. N. (1945). Geomorphology and structure of the East Kaibab
990 Monocline, Arizona and Utah. *Bull. geol. Soc. Am.* 56, 107-150
- 991 Bailey, W. R., Walsh, J. J., & Manzocchi, T. (2005). Fault populations, strain distribution and
992 basement fault reactivation in the East Pennines Coalfield, UK. *Journal of Structural*
993 *Geology*, 27(5), 913–928. <https://doi.org/10.1016/j.jsg.2004.10.014>
- 994 Balsamo, F., Clemenzi, L., Storti, F., Mozafari, M., Solum, J., Swennen, R., Taberner, C., &
995 Tueckmantel, C. (2016). Anatomy and paleofluid evolution of laterally restricted
996 extensional fault zones in the jabal qusaybah anticline, salakh arch, oman. *Bulletin of the*
997 *Geological Society of America*, 128(5–6), 957–972. <https://doi.org/10.1130/B31317.1>
- 998 Baudon, C., & Cartwright, J. (2008). The kinematics of reactivation of normal faults using
999 high resolution throw mapping. *Journal of Structural Geology*, 30(8), 1072–1084.
1000 <https://doi.org/10.1016/j.jsg.2008.04.008>
- 1001 Beck, E., (1929). Salt Creek oil field, Natrona County, Wyoming. In: Structure of Typical
1002 American Oilfields II. The American Association of Petroleum Geologists, pp. 589–
1003 603
- 1004 Bell, F.G., (2000). Engineering Properties of Rocks, 4th ed. Blackwell, Oxford.

- 1005 Bond, D. C., Atherton, E., Bristol, H. M., Buschbach, T. C., Stevenson, D. L., Becker, L. E.,
 1006 Dawson, T. A., Fernald, E. C., Schwalb, H., Wilson, E. N., Statler, A. T., Stearns, R. G.
 1007 & Buehner, J. H. (1971). Possible future petroleum potential of Region 9--Illinois Basin,
 1008 Cincinnati Arch, and Northern Mississippi Embayment. In: Future Petroleum Provinces
 1009 of the United States-- Their Geology and Potential (edited by Cram, I. H.). Am. Ass.
 1010 Petrol. Geol. Memoir 15, 1165-1218.
- 1011 Bramham, E. K., Wright, T. J., Paton, D. A., & Hodgson, D. M. (2021). A new model for the
 1012 growth of normal faults developed above pre-existing structures. *Geology*, 49(5), 587–
 1013 591. <https://doi.org/10.1130/G48290.1>
- 1014 Brunstrom, R. G. W. (1963). Recently discovered oilfields in Britain. *World Petroleum*
 1015 *Congress Proceedings, 1963-June*, 11–20.
- 1016 Cartwright, J.A., Mansfield, C., Trudgill, B., (1996). The growth of normal faults by segment
 1017 linkage. In: Buchanan, P.G., Nieuwland, P.G. (Eds.), *Modern Developments in*
 1018 *Structural Interpretation, Validation and Modelling* Special Publication of the
 1019 Geological Society of London, 99, pp. 163–177.
- 1020 Cartwright, J. A., Trudgill, B. D., & Mansfield, C. S. (1995). Fault growth by segment
 1021 linkage: an explanation for scatter in maximum displacement and trace length data from
 1022 the Canyonlands Grabens of SE Utah. *Journal of Structural Geology*, 17(9), 1319–1326.
 1023 [https://doi.org/10.1016/0191-8141\(95\)00033-A](https://doi.org/10.1016/0191-8141(95)00033-A)
- 1024 Cave, R. (1977). Geology of the Malmestry District. Mem. geol. Surv. Gt Br., sheet 251
- 1025 Childs, C., Manzocchi, T., Nicol, A., Walsh, J. J., Soden, A. M., Conneally, J. C., &
 1026 Delogkos, E. (2017a). The relationship between normal drag, relay ramp aspect ratio and
 1027 fault zone structure. *Geological Society Special Publication*, 439, 355–372.
 1028 <https://doi.org/10.1144/SP439.16>
- 1029 Childs, C., Holdsworth, R. E., Jackson, C. A. L., Manzocchi, T., Walsh, J. J., & Yielding, G.
 1030 (2017b). Introduction to the geometry and growth of normal faults. *Geological Society*
 1031 *Special Publication*, 439(1), 1–9. <https://doi.org/10.1144/SP439.24>
- 1032 Clark, R. M., & Cox, S. J. D. (1996). A modern regression approach to determining fault
 1033 displacement-length scaling relationships. *Journal of Structural Geology*, 18(2–3), 147–
 1034 152. [https://doi.org/10.1016/S0191-8141\(96\)80040-X](https://doi.org/10.1016/S0191-8141(96)80040-X)
- 1035 Cowie, P. A., & Scholz, C. H. (1992a). Displacement-length scaling relationship for faults:
 1036 data synthesis and discussion. *Journal of Structural Geology*, 14(10), 1149–1156.
 1037 [https://doi.org/10.1016/0191-8141\(92\)90066-6](https://doi.org/10.1016/0191-8141(92)90066-6)
- 1038 Cowie, P. A., & Scholz, C. H. (1992b). Physical explanation for the displacement-length
 1039 relationship of faults using a post-yield fracture mechanics model. *Journal of Structural*
 1040 *Geology*, 14(10), 1133–1148. [https://doi.org/10.1016/0191-8141\(92\)90065-5](https://doi.org/10.1016/0191-8141(92)90065-5)

- 1041 Crider, J. G., & Pollard, D. D. (1998). Fault linkage: Three-dimensional mechanical
1042 interaction between echelon normal faults. *Journal of Geophysical Research: Solid*
1043 *Earth*, 103(10), 24373–24391. <https://doi.org/10.1029/98jb01353>
- 1044 Davarpanah, S. M., Vasarhelyi, B., & Török, Á. (2020). Technical Note: Determination of
1045 Young's Modulus and Poisson's Ratio for Intact Stratified Rocks and their Relationship
1046 with Uniaxial Compressive Strength. *Australian Geomechanics Journal*, 55(4), 101–
1047 118.
- 1048 Davis, K., Burbank, D.W., Fisher, D., Wallaces, S., Nobes, D., (2005). Thrust-fault growth
1049 and segment linkage in the active Ostler fault zone, New Zealand. *Journal of Structural*
1050 *Geology* 27, 1528-1546
- 1051 Davison, I., (1994). Linked fault systems; extensional, strike-slip and contractional. In:
1052 Hancock, P.L. (Ed.), *Continental Deformation*. Pergamon Press, pp. 121–142.
- 1053 Dawers, N. H., Anders, M. H., & Scholz, C. H. (1993). Growth of normal faults:
1054 displacement-length scaling. In *Geology* (Vol. 21, Issue 12, pp. 1107–1110).
1055 [https://doi.org/10.1130/0091-7613\(1993\)021<1107:GONFDL>2.3.CO;2](https://doi.org/10.1130/0091-7613(1993)021<1107:GONFDL>2.3.CO;2)
- 1056 Dawers, N. H., & Anders, M. H. (1995). Displacement-length scaling and fault linkage.
1057 *Journal of Structural Geology*, 17(5), 607–614.
- 1058 Delogkos, E., Manzocchi, T., Childs, C., Sachanidis, C., Barbas, T., Schöpfer, M. P. J.,
1059 Chatzipetros, A., Pavlides, S., & Walsh, J. J. (2017). Throw partitioning across normal
1060 fault zones in the Ptolemais Basin, Greece. *Geological Society Special Publication*,
1061 439(1), 333–353. <https://doi.org/10.1144/SP439.19>
- 1062 Delogkos, E., Mudasar Saqab, M., J. Walsh, J., Roche, V., & Childs, C. (2020). Throw
1063 variations and strain partitioning associated with fault-bend folding along normal faults.
1064 *Solid Earth*, 11(3), 935–945. <https://doi.org/10.5194/se-11-935-2020>
- 1065 Densmore, A. L. (2004). Footwall topographic development during continental extension.
1066 *Journal of Geophysical Research*, 109(F3), 1–16. <https://doi.org/10.1029/2003jf000115>
- 1067 Dobson, P., & Houseworth, J. (2013). *Inventory of Shale Hydrological, and Including*
1068 *Geologic, Formations in the US Mechanical Characteristics*.
- 1069 Drozdowski, V. G. (1980). Tiefenteknik der Emscher- und Essener-Hauptmulde im
1070 mittleren Ruhrgebiet. In: *Beiträge zur Tieftektonik des Ruhrkarbons*. Geologisches
1071 Laudesaint Nordrein-Westfalen, Krefeld, 45-83.
- 1072 Duffy, O. B., Nixon, C. W., Bell, R. E., Jackson, C. A. L., Gawthorpe, R. L., Sanderson, D.
1073 J., & Whipp, P. S. (2017). The topology of evolving rift fault networks: Single-phase vs
1074 multi-phase rifts. *Journal of Structural Geology*, 96, 192–202.
1075 <https://doi.org/10.1016/j.jsg.2017.02.001>
- 1076 Elliott, D. (1976). The Energy Balance and Deformation Mechanisms of Thrust Sheets.
1077 *Philosophical Transactions of the Royal Society A: Mathematical, Physical and*
1078 *Engineering Sciences*, 283(1312), 289–312.

- 1079 Ellis, M. A., & Barnes, J. B. (2015). A global perspective on the topographic response to fault
1080 growth. *Geosphere*, 11(4), 1008–1023. <https://doi.org/10.1130/GES01156.1>
- 1081 Faure Walker, J. P., Roberts, G. P., Cowie, P. A., Papanikolaou, I. D., Sammonds, P. R.,
1082 Michetti, A. M., & Phillips, R. J. (2009). Horizontal strain-rates and throw-rates across
1083 breached relay zones, central Italy: Implications for the preservation of throw deficits at
1084 points of normal fault linkage. *Journal of Structural Geology*, 31(10), 1145–1160.
1085 <https://doi.org/10.1016/j.jsg.2009.06.011>
- 1086 Finch, E., & Gawthorpe, R. (2017). Growth and interaction of normal faults and fault
1087 network evolution in rifts: Insights from three-dimensional discrete element modelling.
1088 *Geological Society Special Publication*, 439(1), 219–248.
1089 <https://doi.org/10.1144/SP439.23>
- 1090 Fintland, T. W. (2011). *Measurements of Young's Modulus on Rock Samples at Small*
1091 *Amplitude and Low Frequency*.
- 1092 Fossen, H., Hesthammer, J., (1998). Deformation bands and their significance in porous
1093 sandstone reservoirs. *First Break* 16, 21–25.
- 1094 Fossen, H., & Rotevatn, A. (2012). Characterization of deformation bands associated with
1095 normal and reverse stress states in the Navajo Sandstone, Utah: Discussion. *AAPG*
1096 *Bulletin*, 96(5), 869–876. <https://doi.org/10.1306/09221110173>
- 1097 Fossen, H., & Rotevatn, A. (2016). Fault linkage and relay structures in extensional settings-
1098 A review. *Earth-Science Reviews*, 154, 14–28.
1099 <https://doi.org/10.1016/j.earscirev.2015.11.014>
- 1100 Fox, F.G., (1959). Structure and accumulation of hydrocarbon in southern Foothills, Alberta,
1101 Canada. *Bulletin of the American Association of Petroleum Geologists* 43, 992–1025
- 1102 Freeman, B., Boulton, P. J., Yielding, G., & Menpes, S. (2010). Using empirical geological
1103 rules to reduce structural uncertainty in seismic interpretation of faults. *Journal of*
1104 *Structural Geology*, 32(11), 1668–1676. <https://doi.org/10.1016/j.jsg.2009.11.001>
- 1105 Freund, R., (1970). Rotation of strike slip faults in Sistan, southeast Iran. *Journal of Geology*
1106 78, 188–200
- 1107 Frost, D. V. & Halliday, D. W. (1980). Geology of the country around Bellingham. Mem.
1108 geol. Surv. Gt Br., sheet 13
- 1109 Frost, D. V. & Smart, J. G. O. (1979). Geology of the country north of Derby. Mere. geol.
1110 Surv. Gt Br., sheet 125
- 1111 Gauthier, B. D. M., & Lake, S. D. (1993). Probabilistic modeling of faults below the limit of
1112 seismic resolution in Pelican Field, North Sea, offshore United Kingdom. In *American*
1113 *Association of Petroleum Geologists Bulletin* (Vol. 77, Issue 5, pp. 761–777).
1114 <https://doi.org/10.1306/bdff8d4e-1718-11d7-8645000102c1865d>

- 1115 Gercek, H. (2007). Poisson's ratio values for rocks. *International Journal of Rock Mechanics*
1116 *and Mining Sciences*, 44(1), 1–13. <https://doi.org/10.1016/j.ijrmms.2006.04.011>
- 1117 Ghalayini, R., Homberg, C., Daniel, J. M., & Nader, F. H. (2017). Growth of layer-bound
1118 normal faults under a regional anisotropic stress field. *Geological Society Special*
1119 *Publication*, 439(1), 57–78. <https://doi.org/10.1144/SP439.13>
- 1120 Giba, M., Walsh, J. J., & Nicol, A. (2012). Segmentation and growth of an obliquely
1121 reactivated normal fault. *Journal of Structural Geology*, 39, 253–267.
1122 <https://doi.org/10.1016/j.jsg.2012.01.004>
- 1123 Gillespie, P.A., (1991). Structural analysis of faults and folds with examples from the South
1124 Wales Coalfield and Ruhr Coalfield. Unpublished PhD thesis, University of Wales.
- 1125 Gillespie, P. A., Howard, C. B., Walsh, J. J., & Watterson, J. (1993). Measurement and
1126 characterisation of spatial distributions of fractures. *Tectonophysics*, 226, 113–141.
1127 <https://doi.org/10.1021/jo00120a014>
- 1128 Gillespie, P. A., Walsh, J. J., & Watterson, J. (1992). Limitations of dimension and
1129 displacement data from single faults and the consequences for data analysis and
1130 interpretation. *Journal of Structural Geology*, 14(10), 1157–1172.
1131 [https://doi.org/10.1016/0191-8141\(92\)90067-7](https://doi.org/10.1016/0191-8141(92)90067-7)
- 1132 Gross, M. R., Gutiérrez-Alonso, G., Bai, T., Wacker, M. A., Collinsworth, K. B., & Behl, R.
1133 J. (1997). Influence of mechanical stratigraphy and kinematics on fault scaling relations.
1134 *Journal of Structural Geology*, 19(2), 171–183. [https://doi.org/10.1016/S0191-](https://doi.org/10.1016/S0191-8141(96)00085-5)
1135 [8141\(96\)00085-5](https://doi.org/10.1016/S0191-8141(96)00085-5)
- 1136 Gudmundsson, A. (2004). Effects of Young's modulus on fault displacement. *Comptes*
1137 *Rendus - Geoscience*, 336(1), 85–92. <https://doi.org/10.1016/j.crte.2003.09.018>
- 1138 Hedtmann, N., & Alber, M. (2017). Investigation of Water-permeability and Ultrasonic Wave
1139 Velocities of German Malm Aquifer Rocks for Hydro-Geothermal Energy. *Procedia*
1140 *Engineering*, 191(June), 127–133. <https://doi.org/10.1016/j.proeng.2017.05.163>
- 1141 Hemelsdaël, R., & Ford, M. (2016). Relay zone evolution: A history of repeated fault
1142 propagation and linkage, central Corinth rift, Greece. *Basin Research*, 28(1), 34–56.
1143 <https://doi.org/10.1111/bre.12101>
- 1144 Henstra, G. A., Rotevatn, A., Gawthorpe, R. L., & Ravnås, R. (2015). Evolution of a major
1145 segmented normal fault during multiphase rifting: The origin of plan-view zigzag
1146 geometry. *Journal of Structural Geology*, 74, 45–63.
1147 <https://doi.org/10.1016/j.jsg.2015.02.005>
- 1148 Hollinsworth, A. D., Koehn, D., Dempster, T. J., & Aanyu, K. (2019). Structural controls on
1149 the interaction between basin fluids and a rift flank fault: Constraints from the Bwamba
1150 Fault, East African Rift. *Journal of Structural Geology*, 118(November 2018), 236–249.
1151 <https://doi.org/10.1016/j.jsg.2018.10.012>

- 1152 Huntoon, P. (1974). *The Post-Paleozoic Structural Geology of the Eastern Grand Canyon,*
1153 *Arizona.*
- 1154 Iezzi, F., Mildon, Z., Walker, J. F., Roberts, G., Goodall, H., Wilkinson, M., & Robertson, J.
1155 (2018). Coseismic Throw Variation Across Along-Strike Bends on Active Normal
1156 Faults: Implications for Displacement Versus Length Scaling of Earthquake Ruptures.
1157 *Journal of Geophysical Research: Solid Earth*, 123(11), 9817–9841.
1158 <https://doi.org/10.1029/2018JB016732>
- 1159 Jackson, C. A. L., Bell, R. E., Rotevatn, A., & Tvedt, A. B. M. (2017). Techniques to
1160 determine the kinematics of synsedimentary normal faults and implications for fault
1161 growth models. *Geological Society Special Publication*, 439(1), 187–217.
1162 <https://doi.org/10.1144/SP439.22>
- 1163 Jackson, C. A. L., & Rotevatn, A. (2013). 3D seismic analysis of the structure and evolution
1164 of a salt-influenced normal fault zone: A test of competing fault growth models. *Journal*
1165 *of Structural Geology*, 54, 215–234. <https://doi.org/10.1016/j.jsg.2013.06.012>
- 1166 Jackson, J., Norris, R., & Youngson, J. (1996). The structural evolution of active fault and
1167 fold systems in central Otago, New Zealand: Evidence revealed by drainage patterns.
1168 *Journal of Structural Geology*, 18(2–3), 217–234. [https://doi.org/10.1016/S0191-](https://doi.org/10.1016/S0191-8141(96)80046-0)
1169 [8141\(96\)80046-0](https://doi.org/10.1016/S0191-8141(96)80046-0)
- 1170 Janoschek, R. H. & Gotzinger, K. G. H. (1969). Exploration for oil and gas in Austria. In: *The*
1171 *Exploration for Petroleum in Europe and North Africa* (edited by Hepple, P.). Elsevier,
1172 Amsterdam, 161–180
- 1173 Karp, T., Scholz, C. A., & McGlue, M. M. (2012). Structure and stratigraphy of the Lake
1174 Albert rift, East Africa: Observations from seismic reflection and gravity data. *AAPG*
1175 *Memoir*, 95(August), 299–318. <https://doi.org/10.1306/13291394M952903>
- 1176 Khalil, S. M., & McClay, K. R. (2017). 3D geometry and kinematic evolution of extensional
1177 fault-related folds, NW Red Sea, Egypt. *Geological Society Special Publication*, 439(1),
1178 109–130. <https://doi.org/10.1144/SP439.11>
- 1179 Kim, Y. S., Andrews, J. R., & Sanderson, D. J. (2000). Damage zones around strike-slip fault
1180 systems and strike-slip fault evolution, Crackington Haven, southwest England.
1181 *Geosciences Journal*, 4(2), 53–72. <https://doi.org/10.1007/BF02910127>
- 1182 Kim, Y. S., & Sanderson, D. J. (2005). The relationship between displacement and length of
1183 faults: A review. *Earth-Science Reviews*, 68(3–4), 317–334.
1184 <https://doi.org/10.1016/j.earscirev.2004.06.003>
- 1185 Kicono, L. (2005). *The Semliki Basin, Uganda: Its sedimentation history and stratigraphy in*
1186 *relation to petroleum accumulation.* University of Cape Town.
- 1187 Kolyukhin, D., & Torabi, A. (2012). Statistical analysis of the relationships between faults
1188 attributes. *Journal of Geophysical Research: Solid Earth*, 117(5), 1–14.
1189 <https://doi.org/10.1029/2011JB008880>

- 1190 Krantz, R. W. (1988). Multiple fault sets and three-dimensional strain: Theory and
 1191 application. *Journal of Structural Geology*, 10(3), 225–237.
 1192 [https://doi.org/10.1016/0191-8141\(88\)90056-9](https://doi.org/10.1016/0191-8141(88)90056-9)
- 1193 Lamarche, G., Proust, J. N., & Nodder, S. D. (2005). Long-term slip rates and fault
 1194 interactions under low contractional strain, Wanganui Basin, New Zealand. *Tectonics*,
 1195 24(4), 1–30. <https://doi.org/10.1029/2004TC001699>
- 1196 Lathrop, B. A., Jackson, C. A. L., Bell, R. E., & Rotevatn, A. (2021). Normal Fault
 1197 Kinematics and the Role of Lateral Tip Retreat: An Example From Offshore NW
 1198 Australia. *Tectonics*, 40(5). <https://doi.org/10.1029/2020TC006631>
- 1199 Liang, W., Yang, C., Zhao, Y., Dusseault, M. B., & Liu, J. (2007). Experimental
 1200 investigation of mechanical properties of bedded salt rock. *International Journal of Rock*
 1201 *Mechanics and Mining Sciences*, 44(3), 400–411.
 1202 <https://doi.org/10.1016/j.ijrmms.2006.09.007>
- 1203 MacMillan, R. A. (1975), The orientation and sense of displacement of strike-slip faults in
 1204 continental crust, BS thesis, Carleton Univ., Ottawa, Ont., Canada.
- 1205 Małkowski, P., Ostrowski, L., & Brodny, J. (2018). Analysis of Young’s modulus for
 1206 Carboniferous sedimentary rocks and its relationship with uniaxial compressive strength
 1207 using different methods of modulus determination. *Journal of Sustainable Mining*,
 1208 17(3), 145–157. <https://doi.org/10.1016/j.jsm.2018.07.002>
- 1209 Marrett, R., & Allmendinger, R. W. (1991). Estimates of strain due to brittle faulting:
 1210 sampling of fault populations. *Journal of Structural Geology*, 13(6), 735–738.
 1211 [https://doi.org/10.1016/0191-8141\(91\)90034-G](https://doi.org/10.1016/0191-8141(91)90034-G)
- 1212 Mayuga, M. (1970). Geology and development of California’s giant--Wilmington oil field.
 1213 *American Association of Petroleum Geologists, Memoir 14*, 158–184.
 1214 <http://archives.datapages.com/data/specpubs/fieldst2/data/a009/a009/0001/0150/0158.htm>
 1215 m
- 1216 McClymont, A. F., Villamor, P., & Green, A. G. (2009). Fault displacement accumulation
 1217 and slip rate variability within the Taupo Rift (New Zealand) based on trench and 3-D
 1218 ground-penetrating radar data. *Tectonics*, 28(4), 1–25.
 1219 <https://doi.org/10.1029/2008TC002334>
- 1220 McGlue, M. M., Scholz, C. A., Karp, T., Ongodia, B., & Lezzar, K. E. (2006). Facies
 1221 architecture of flexural margin lowstand delta deposits in Lake Edward, East African rift:
 1222 Constraints from seismic reflection imaging. *Journal of Sedimentary Research*, 76(6),
 1223 942–958. <https://doi.org/10.2110/jsr.2006.068>
- 1224 McGrath, A. (1992). Fault propagation and growth; a study of the Triassic and Jurassic from
 1225 Watchet and Kilve, North Somerset [Master’s thesis]: London, Royal Holloway,
 1226 University of London, 165
- 1227 McLeod, A. E., Dawers, N. H., & Underhill, J. R. (2000). The propagation and linkage of
 1228 normal faults: Insights from the Strathspey-Brent-Stafford fault array, Northern North

- 1229 Sea. *Basin Research*, 12(3–4), 263–284. <https://doi.org/10.1111/j.1365->
1230 2117.2000.00124.x
- 1231 MFRG (Minor Faults Research Group) (1973). A minor fault system around the Otaki area,
1232 Boso Peninsula, Japan. *Earth Science (Chikyu Kagaku)* 27, 180–187
- 1233 Meyer, V., Nicol, A., Childs, C., Walsh, J. J., & Watterson, J. (2002). Progressive localisation
1234 of strain during the evolution of a normal fault population. *Journal of Structural*
1235 *Geology*, 24(8), 1215–1231. [https://doi.org/10.1016/S0191-8141\(01\)00104-3](https://doi.org/10.1016/S0191-8141(01)00104-3)
- 1236 =
- 1237 Morley, C. K., Gabdi, S., & Seusutthiya, K. (2007). Fault superimposition and linkage
1238 resulting from stress changes during rifting: Examples from 3D seismic data,
1239 Phitsanulok Basin, Thailand. *Journal of Structural Geology*, 29(4), 646–663.
1240 <https://doi.org/10.1016/j.jsg.2006.11.005>
- 1241 Morley, C. K. (2017). The impact of multiple extension events, stress rotation and inherited
1242 fabrics on normal fault geometries and evolution in the Cenozoic rift basins of Thailand.
1243 *Geological Society Special Publication*, 439(1), 413–445.
1244 <https://doi.org/10.1144/SP439.3>
- 1245 Morley, C. K., Nelson, R. A., Patton, T. L., & Munn, S. G. (1990). Transfer zones in the East
1246 African rift system and their relevance to hydrocarbon exploration in rifts. *American*
1247 *Association of Petroleum Geologists Bulletin*, 74(8), 1234–1253.
1248 <https://doi.org/10.1306/0c9b2475-1710-11d7-8645000102c1865d>
- 1249 Morley, C. K. (2002). Evolution of large normal faults: Evidence from seismic reflection
1250 data. *AAPG Bulletin*, 86(6), 961–978. <https://doi.org/10.1002/2016GC006582.Subsea>
- 1251 Mouslopoulou, V., Walsh, J. J., & Nicol, A. (2009). Fault displacement rates on a range of
1252 timescales. *Earth and Planetary Science Letters*, 278(3–4), 186–197.
1253 <https://doi.org/10.1016/j.epsl.2008.11.031>
- 1254 Muraoka, H., & Kamata, H. (1983). Displacement distribution along minor fault traces.
1255 *Journal of Structural Geology*, 5(5), 483–495. <https://doi.org/10.1016/0191->
1256 8141(83)90054-8
- 1257 Nelson, P. H. H. (1980). Role of reflection seismic in development of Nembe Creek Field,
1258 Nigeria. In: *Giant Oil and Gas Fields of the Decade: 1968-1978* (edited by Halbouty,
1259 M. T.). Am. Ass. Petrol. Geol., Memoir 30, 565-576.
- 1260 Nicol, A., Childs, C., Walsh, J. J., Manzocchi, T., & Schöpfer, M. P. J. (2017). Interactions
1261 and growth of faults in an outcrop-scale system. *Geological Society Special Publication*,
1262 439, 23–39. <https://doi.org/10.1144/SP439.9>
- 1263 Nicol, A., Walsh, J. J., Villamor, P., Seebeck, H., & Berryman, K. R. (2010). Normal fault
1264 interactions, paleoearthquakes and growth in an active rift. *Journal of Structural*
1265 *Geology*, 32(8), 1101–1113. <https://doi.org/10.1016/j.jsg.2010.06.018>

- 1266 Nicol, A., Watterson, J., Walsh, J. J., & Childs, C. (1996). The shapes, major axis
1267 orientations and displacement patterns of fault surfaces. *Journal of Structural Geology*,
1268 18(2–3), 235–248. [https://doi.org/10.1016/S0191-8141\(96\)80047-2](https://doi.org/10.1016/S0191-8141(96)80047-2)
- 1269 Nicol, A., Walsh, J., Berryman, K., & Nodder, S. (2005). Growth of a normal fault by the
1270 accumulation of slip over millions of years. *Journal of Structural Geology*, 27(2), 327–
1271 342. <https://doi.org/10.1016/j.jsg.2004.09.002>
- 1272 Nicol, A., Walsh, J., Childs, C., & Manzocchi, T. (2020). The growth of faults. In
1273 *Understanding Faults: Detecting, Dating, and Modeling*. Elsevier Inc.
1274 <https://doi.org/10.1016/B978-0-12-815985-9.00006-0>
- 1275 Norcliffe, J., Magee, C., Jackson, C. A. L., Kopping, J., & Lathrop, B. (2021). Fault inversion
1276 contributes to ground deformation above inflating igneous sills. *Volcanica*, 4(1), 1–21.
1277 <https://doi.org/10.30909/VOL.04.01.0121>
- 1278 Opheim, J. A., & Gudmundsson, A. (1989). Formation and geometry of fractures, and related
1279 volcanism, of the Krafla fissure swarm, northeast Iceland. *Geological Society of*
1280 *America Bulletin*, 101(12), 1608–1622. [https://doi.org/10.1130/0016-](https://doi.org/10.1130/0016-7606(1989)101<1608:FAGOFA>2.3.CO;2)
1281 [7606\(1989\)101<1608:FAGOFA>2.3.CO;2](https://doi.org/10.1130/0016-7606(1989)101<1608:FAGOFA>2.3.CO;2)
- 1282 Pan, S., Bell, R. E., Jackson, C. A. L., & Naliboff, J. (2021). Evolution of normal fault
1283 displacement and length as continental lithosphere stretches. *Basin Research*, August.
1284 <https://doi.org/10.1111/bre.12613>
- 1285 Peacock, D. C. P. (1991). Displacement and segment linkage in strike- slip fault zones. *J.*
1286 *Struct. Geol.* 13, 1025-1035. [https://doi.org/10.1016/0191-8141\(91\)90054-M](https://doi.org/10.1016/0191-8141(91)90054-M)
- 1287 Peacock, D. C. P., & Sanderson, D. J. (1991). Displacements, segment linkage and relay
1288 ramps in normal fault zones. *Journal of Structural Geology*, 13(6), 721–733.
1289 [https://doi.org/10.1016/0191-8141\(91\)90033-F](https://doi.org/10.1016/0191-8141(91)90033-F)
- 1290 Peacock, D. C. P., & Sanderson, D. J. (1992). Effects of layering and anisotropy on fault
1291 geometry. *Journal - Geological Society (London)*, 149(5), 793–802.
1292 <https://doi.org/10.1144/gsjgs.149.5.0793>
- 1293 Pickering, G., Peacock, D. C. P., Sanderson, D. J., & Bull, J. M. (1997). Modeling tip zones
1294 to predict the throw and length characteristics of faults. *AAPG Bulletin*, 81(1), 82–99.
1295 <https://doi.org/10.1306/522b4299-1727-11d7-8645000102c1865d>
- 1296 Poulimenos, G. (2000). Scaling properties of normal fault populations in the western Corinth
1297 Graben, Greece: Implications for fault growth in large strain settings. *Journal of*
1298 *Structural Geology*, 22(3), 307–322. [https://doi.org/10.1016/S0191-8141\(99\)00152-2](https://doi.org/10.1016/S0191-8141(99)00152-2)
- 1299 Reeves, J. R. (1929). El Dorado oil field, Butler County, Kansas. Structure of Typical
1300 American Oilfields, Vol. II. Am. Ass. Petrol. Geol., 160-167.
- 1301 Reeve, M. T., Bell, R. E., Duffy, O. B., Jackson, C. A. L., & Sansom, E. (2015). The growth
1302 of non-colinear normal fault systems; What can we learn from 3D seismic reflection

- 1303 data? *Journal of Structural Geology*, 70, 141–155.
 1304 <https://doi.org/10.1016/j.jsg.2014.11.007>
- 1305 Reilly, C., Nicol, A., & Walsh, J. (2017). Importance of pre-existing fault size for the
 1306 evolution of an inverted fault system. *Geological Society Special Publication*, 439(1),
 1307 447–463. <https://doi.org/10.1144/SP439.2>
- 1308 Rioseco, E. M., Löhken, J., Schellschmidt, R., & Tischner, T. (2013). 3-D Geomechanical
 1309 Modeling of the Stress Field in the North German Basin: Case Study Genesys-Borehole
 1310 Gt1 in Hanover Groß-Buchholz. *Proceedings of the Thirty-Eighth Workshop on*
 1311 *Geothermal Reservoir Engineering*.
- 1312 Rippon, J. H. (1985). Contoured patterns of the throw and hade of normal faults in the Coal
 1313 Measures (Westphalian) of north-east Derbyshire (England). *Proceedings - Yorkshire*
 1314 *Geological Society*, 45(3), 147–161. <https://doi.org/10.1144/pygs.45.3.147>
- 1315 Roberts, G. P., & Michetti, A. M. (2004). Spatial and temporal variations in growth rates
 1316 along active normal fault systems: An example from The Lazio-Abruzzo Apennines,
 1317 central Italy. *Journal of Structural Geology*, 26(2), 339–376.
 1318 [https://doi.org/10.1016/S0191-8141\(03\)00103-2](https://doi.org/10.1016/S0191-8141(03)00103-2)
- 1319 Roche, V., Homberg, C., David, C., & Rocher, M. (2014). Normal faults, layering and elastic
 1320 properties of rocks. *Tectonophysics*, 622, 96–109.
 1321 <https://doi.org/10.1016/j.tecto.2014.03.006>
- 1322 Roche, V., Homberg, C., & Rocher, M. (2013). Fault nucleation, restriction, and aspect ratio
 1323 in layered sections: Quantification of the strength and stiffness roles using numerical
 1324 modeling. *Journal of Geophysical Research: Solid Earth*, 118(8), 4446–4460.
 1325 <https://doi.org/10.1002/jgrb.50279>
- 1326 Roche, V., Homberg, C., Van Der Baan, M., & Rocher, M. (2017). Widening of normal fault
 1327 zones due to the inhibition of vertical propagation. *Geological Society Special*
 1328 *Publication*, 439(1), 271–288. <https://doi.org/10.1144/SP439.5>
- 1329 Rotevatn, A., & Fossen, H. (2011). Simulating the effect of subseismic fault tails and process
 1330 zones in a siliciclastic reservoir analogue: Implications for aquifer support and trap
 1331 definition. *Marine and Petroleum Geology*, 28(9), 1648–1662.
 1332 <https://doi.org/10.1016/j.marpetgeo.2011.07.005>
- 1333 Rotevatn, A., Jackson, C. A. L., Tvedt, A. B. M., Bell, R. E., & Blækkan, I. (2019). How do
 1334 normal faults grow? *Journal of Structural Geology*, 125(August 2018), 174–184.
 1335 <https://doi.org/10.1016/j.jsg.2018.08.005>
- 1336 Rowan, M. G. (1997). Three-dimensional geometry and evolution of a segmented detachment
 1337 fold, Mississippi Fan foldbelt, Gulf of Mexico. *Journal of Structural Geology*, 19(3-4
 1338 SPEC. ISS.), 463–480. [https://doi.org/10.1016/s0191-8141\(96\)00098-3](https://doi.org/10.1016/s0191-8141(96)00098-3)
- 1339 Ruzhich, V.V., (1977). Relations between fault parameters and practical application of them.
 1340 In: Mekhanizmy Struktur Vostochonchnoisibiri Novisibirsk (in Russian).

- 1341 Santi, P. M., Holschen, J. E., & Stephenson, R. W. (2000). Improving elastic modulus
1342 measurements for rock based on geology. *Environmental and Engineering Geoscience*,
1343 6(4), 333–346. <https://doi.org/10.2113/gseegeosci.6.4.333>
- 1344 Schlagenhauf, A., Manighetti, I., Malavieille, J., & Dominguez, S. (2008). Incremental
1345 growth of normal faults: Insights from a laser-equipped analog experiment. *Earth and*
1346 *Planetary Science Letters*, 273(3–4), 299–311.
1347 <https://doi.org/10.1016/j.epsl.2008.06.042>
- 1348 Schlische, R. W., Young, S. S., Ackermann, R. V., & Gupta, A. (1996). Geometry and
1349 scaling relations of a population of very small rift-related normal faults. *Geology*, 24(8),
1350 683–686. [https://doi.org/10.1130/0091-7613\(1996\)024<0683:GASROA>2.3.CO;2](https://doi.org/10.1130/0091-7613(1996)024<0683:GASROA>2.3.CO;2)
- 1351 Scholz, C. H., Dawers, N. H., Yu, J. Z., Anders, M. H., & Cowie, P. A. (1993). Fault growth
1352 and fault scaling laws: preliminary results. *Journal of Geophysical Research*, 98(B12),
1353 21951–21961. <https://doi.org/10.1029/93jb01008>
- 1354 Scholz, C. A., Shillington, D. J., Wright, L. J. M., Accardo, N., Gaherty, J. B., &
1355 Chindandali, P. (2020). Intrarift fault fabric, segmentation, and basin evolution of the
1356 Lake Malawi (Nyasa) Rift, East Africa. *Geosphere*, 16(5), 1293–1311.
1357 <https://doi.org/10.1130/GES02228.1>
- 1358 Schultz, R. A., & Fossen, H. (2002). Displacement-length scaling in three dimensions: The
1359 importance of aspect ratio and application to deformation bands. *Journal of Structural*
1360 *Geology*, 24(9), 1389–1411. [https://doi.org/10.1016/S0191-8141\(01\)00146-8](https://doi.org/10.1016/S0191-8141(01)00146-8)
- 1361 Schultz, R. A., Soliva, R., Fossen, H., Okubo, C. H., & Reeves, D. M. (2008). Dependence of
1362 displacement-length scaling relations for fractures and deformation bands on the
1363 volumetric changes across them. *Journal of Structural Geology*, 30(11), 1405–1411.
1364 <https://doi.org/10.1016/j.jsg.2008.08.001>
- 1365 Shepherd, J., & Burns, K. L. (1978). Fault Swarms in the Greta Coal Seam, New South
1366 Wales. *Proc Australas Inst Min Metall*, 267, 27–36.
- 1367 Shoemaker, E. M., Squires, R. L. & Abrams, M. J. (1978). Bright Angel and Mesa Butte fault
1368 systems of northern Arizona. In: *Cenozoic Tectonics and Regional Geophysics of the*
1369 *Western Cordillera* (edited by Smith, R. B. & Eaton, G. P.). Geol. Soc. Am. Memoir
1370 152,341-367.
- 1371 Shunshan, X., Nieto-Samaniego, A. F., Velasquillo-Martínez, L. G., Grajales-Nishimura, J.
1372 M., Murillo-Muñetón, G., & García-Hernández, J. (2011). Factors influencing the fault
1373 displacement-length relationship: An example from the Cantarell oilfield, Gulf of
1374 Mexico. *Geofísica Internacional*, 50(3), 279–293.
1375 <https://doi.org/10.22201/igeof.00167169p.2011.50.3.227>
- 1376 Siegburg, M., Bull, J. M., Nixon, C. W., Keir, D., Gernon, T. M., Corti, G., Abebe, B.,
1377 Sanderson, D. J., & Ayele, A. (2020). Quantitative Constraints on Faulting and Fault
1378 Slip Rates in the Northern Main Ethiopian Rift. *Tectonics*, 39(8).
1379 <https://doi.org/10.1029/2019TC006046>

- 1380 Soliva, R., & Benedicto, A. (2005). A linkage criterion for segmented normal faults. *Journal*
1381 *of Structural Geology*, 26(12), 2251–2267. <https://doi.org/10.1016/j.jsg.2004.06.008>
- 1382 Soliva, R., Benedicto, A., & Maerten, L. (2006). Spacing and linkage of confined normal
1383 faults: Importance of mechanical thickness. *Journal of Geophysical Research: Solid*
1384 *Earth*, 111(1), 1–17. <https://doi.org/10.1029/2004JB003507>
- 1385 Soliva, R., & Schulz, R. A. (2008). Distributed and localized faulting in extensional settings:
1386 Insight from the north Ethiopian Rift-Afar transition area. *Tectonics*, 27(2), 1–19.
1387 <https://doi.org/10.1029/2007TC002148>
- 1388 Taylor, S. K., Nicol, A., & Walsh, J. J. (2008). Displacement loss on growth faults due to
1389 sediment compaction. *Journal of Structural Geology*, 30(3), 394–405.
1390 <https://doi.org/10.1016/j.jsg.2007.11.006>
- 1391 Teas, L. P. (1929). Bellevue oil field, Bossier Parish, Louisiana. In: Structure of Typical
1392 American Oilfields, Vol. II. Am. Ass. Petrol. Geol., 229-253.
- 1393 Torabi, A., Alaei, B., & Libak, A. (2019). Normal fault 3D geometry and displacement
1394 revisited: Insights from faults in the Norwegian Barents Sea. *Marine and Petroleum*
1395 *Geology*, 99(April 2018), 135–155. <https://doi.org/10.1016/j.marpetgeo.2018.09.032>
- 1396 Torabi, A., & Berg, S. S. (2011). Scaling of fault attributes: A review. *Marine and Petroleum*
1397 *Geology*, 28(8), 1444–1460. <https://doi.org/10.1016/j.marpetgeo.2011.04.003>
- 1398 Tschopp, R. H. (1967). Development of the Fahud field. *World Petroleum Congress*
1399 *Proceedings, 1967-April*, 243–250.
- 1400 Tvedt, A. B. M., Rotevatn, A., & Jackson, C. A. L. (2016). Supra-salt normal fault growth
1401 during the rise and fall of a diapir: Perspectives from 3D seismic reflection data,
1402 Norwegian North Sea. *Journal of Structural Geology*, 91, 1–26.
1403 <https://doi.org/10.1016/j.jsg.2016.08.001>
- 1404 Van den Bark, E. & Thomas, O. D. (1980). Ekofisk: First of the Giant Combining (A4) and
1405 (A5) Oil Fields in Western Europe. In: Giant Oil and Gas Fields of the Decade: 1968-
1406 1978 (edited by Halbouty, M.T.). Am. Ass. Petrol. Geol., Memoir 30, 195-224.
- 1407 Verdier, A. C., Oki, A. C. & Suardy, A. (1980). Geology of the Handil Field (East
1408 Kalimantan-Indonesia). In: Giant Oil and Gas Fields of the Decade: 1968--1978 (edited
1409 by Halbouty, M. T.). Am. Ass. Petrol. Geol., Memoir 30, 399-421.
- 1410 Vétel, W., Le Gall, B., & Walsh, J. J. (2005). Geometry and growth of an inner rift fault
1411 pattern: The Kino Sogo Fault Belt, Turkana Rift (North Kenya). *Journal of Structural*
1412 *Geology*, 27(12), 2204–2222. <https://doi.org/10.1016/j.jsg.2005.07.003>
- 1413 Villemain, T., Angelier, J., & Sunwoo, C. (1995). Fractal Distribution of Fault Length and
1414 Offsets: Implications of Brittle Deformation Evaluation—The Lorraine Coal Basin.
1415 *Fractals in the Earth Sciences*, 205–226. https://doi.org/10.1007/978-1-4899-1397-5_10

- 1416 Villemain, T., & Sunwoo, C. (1987). Distribution logarithmique self-similaire des rejets et
1417 longueurs de failles: exemple du bassin houiller Lorrain. *Comptes Rendus de l'Académie*
1418 *Des Sciences. Série 2, Mécanique, Physique, Chimie, Sciences de l'univers, Sciences de*
1419 *La Terre*, 305(16), 1309–1312.
- 1420 Walsh, J. J., Bailey, W. R., Childs, C., Nicol, A., & Bonson, C. G. (2003). Formation of
1421 segmented normal faults: A 3-D perspective. *Journal of Structural Geology*, 25(8),
1422 1251–1262. [https://doi.org/10.1016/S0191-8141\(02\)00161-X](https://doi.org/10.1016/S0191-8141(02)00161-X)
- 1423 Walsh, J. J., Nicol, A., & Childs, C. (2002). An alternative model for the growth of faults.
1424 *Journal of Structural Geology*, 24(11), 1669–1675. [https://doi.org/10.1016/S0191-](https://doi.org/10.1016/S0191-8141(01)00165-1)
1425 [8141\(01\)00165-1](https://doi.org/10.1016/S0191-8141(01)00165-1)
- 1426 Walsh, J. J., & Watterson, J. (1987). Distributions of cumulative displacement and seismic
1427 slip on a single normal fault surface. *Journal of Structural Geology*, 9(8), 1039–1046.
1428 [https://doi.org/10.1016/0191-8141\(87\)90012-5](https://doi.org/10.1016/0191-8141(87)90012-5)
- 1429 Walsh, J. J., & Watterson, J. (1989). Displacement gradients on fault surfaces. *Journal of*
1430 *Structural Geology*, 11(3), 307–316. [https://doi.org/10.1016/0191-8141\(89\)90070-9](https://doi.org/10.1016/0191-8141(89)90070-9)
- 1431 Walsh, J. J., & Watterson, J. (1988). Analysis of the relationship between displacements and
1432 dimensions of faults. *Journal of Structural Geology*, 10(3), 239–247.
1433 [https://doi.org/10.1016/0191-8141\(88\)90057-0](https://doi.org/10.1016/0191-8141(88)90057-0)
- 1434 Watterson, J. (1986). Fault dimensions, displacements and growth. *Pure and Applied*
1435 *Geophysics PAGEOPH*, 124(1–2), 365–373. <https://doi.org/10.1007/BF00875732>
- 1436 Wedmore, L. N. J., Biggs, J., Williams, J. N., Fagereng, Dulanya, Z., Mphepo, F., & Mdala,
1437 H. (2020). Active Fault Scarps in Southern Malawi and Their Implications for the
1438 Distribution of Strain in Incipient Continental Rifts. *Tectonics*, 39(3).
1439 <https://doi.org/10.1029/2019TC005834>
- 1440 Welch, M. J., Davies, R. K., Knipe, R. J., & Tueckmantel, C. (2009). A dynamic model for
1441 fault nucleation and propagation in a mechanically layered section. *Tectonophysics*,
1442 474(3–4), 473–492. <https://doi.org/10.1016/j.tecto.2009.04.025>
- 1443 Wells, D. L., & Coppersmith, Kevin, J. (1994). New empirical relationship between
1444 magnitude, rupture length, rupture width, rupture area, and surface displacement.
1445 *Bulletin of the Seismological Society of America*, 84(4), 974–1002.
- 1446 Whipp, P. S., Jackson, C. A. L., Gawthorpe, R. L., Dreyer, T., & Quinn, D. (2014). Normal
1447 fault array evolution above a reactivated rift fabric; a subsurface example from the
1448 northern Horda Platform, Norwegian North Sea. *Basin Research*, 26(4), 523–549.
1449 <https://doi.org/10.1111/bre.12050>
- 1450 Wibberley, C. A. J., Petit, J. P., & Rives, T. (2000a). Micromechanics of shear rupture and
1451 the control of normal stress. *Journal of Structural Geology*, 22(4), 411–427.
1452 [https://doi.org/10.1016/S0191-8141\(99\)00158-3](https://doi.org/10.1016/S0191-8141(99)00158-3)

- 1453 Wibberley, C. A. J., Petit, J. P., & Rives, T. (2000b). Mechanics of cataclastic “deformation
1454 band” faulting in high-porosity Sandstone, Provence. *Comptes Rendus de l’Academie de
1455 Sciences - Serie IIa: Sciences de La Terre et Des Planetes*, 331(6), 419–425.
1456 [https://doi.org/10.1016/S1251-8050\(00\)01423-3](https://doi.org/10.1016/S1251-8050(00)01423-3)
- 1457 Wibberley, C. A. J., Petit, J. P., & Rives, T. (1999). Mechanics of high displacement gradient
1458 faulting prior to lithification. *Journal of Structural Geology*, 21(3), 251–257.
1459 [https://doi.org/10.1016/S0191-8141\(99\)00006-1](https://doi.org/10.1016/S0191-8141(99)00006-1)
- 1460 Wilkins, S. J., & Gross, M. R. (2002). Normal fault growth in layered rocks at Split
1461 Mountain, Utah: Influence of mechanical stratigraphy on dip linkage, fault restriction
1462 and fault scaling. *Journal of Structural Geology*, 24(9), 1413–1429.
1463 [https://doi.org/10.1016/S0191-8141\(01\)00154-7](https://doi.org/10.1016/S0191-8141(01)00154-7)
- 1464 Willemse, E. J. M. (1997). Segmented normal faults: Correspondence between three-
1465 Dimensional mechanical models and field data. *Journal of Geophysical Research B:
1466 Solid Earth*, 102(B1), 675–692. <https://doi.org/10.1029/96jb01651>
- 1467 Williams, J. N., Fagereng, Å., Wedmore, L., Biggs, J., Mdala, H., Mphepo, F., & Hodge, M.
1468 (2021). Low dissipation of earthquake energy along faults that follow pre-existing
1469 weaknesses: field and microstructural observations of Malawi’s Bilila-Mtakataka Fault.
1470 *Preprint*. <https://doi.org/10.5194/nhess-2021-306>
- 1471 Wood, G.H., Trexler, J.P., Kehn, T.M., (1969). Geology of the west-central part of the
1472 Southern Anthracite field and adjoining areas, Pennsylvania. Geology Survey,
1473 Professional paper.
- 1474 Woodland, A.W., Evans, W.B., (1964). The Geology of the South Wales Coalfield. Part IV.
1475 The Country around Pontypridd and Maesteg. H.M.S.O., London.
- 1476 Worthington, R. P., & Walsh, J. J. (2017). Timing, growth and structure of a reactivated
1477 basin-bounding fault. *Geological Society Special Publication*, 439(1), 511-531.
1478 <https://doi.org/10.1144/SP439.14>
- 1479 Xu, S. S., Nieto-Samaniego, A. F., Alaniz-Álvarez, S. A., & Velasquillo-Martínez, L. G.
1480 (2006). Effect of sampling and linkage on fault length and length-displacement
1481 relationship. *International Journal of Earth Sciences*, 95(5), 841–853.
1482 <https://doi.org/10.1007/s00531-005-0065-3>
- 1483 Xu, H., Zhou, W., Xie, R., Da, L., Xiao, C., Shan, Y., & Zhang, H. (2016). Characterization
1484 of Rock Mechanical Properties Using Lab Tests and Numerical Interpretation Model of
1485 Well Logs. *Mathematical Problems in Engineering*, 2016.
1486 <https://doi.org/10.1155/2016/5967159>
- 1487 Yielding, G., Needham, T., & Jones, H. (1996). Sampling of fault populations using sub-
1488 surface data: A review. *Journal of Structural Geology*, 18(2–3), 135–146.
1489 [https://doi.org/10.1016/S0191-8141\(96\)80039-3](https://doi.org/10.1016/S0191-8141(96)80039-3)
- 1490 Young, M. J., Gawthorpe, R. L., & Hardy, S. (2001). Growth and linkage of a segmented
1491 normal fault zone; the Late Jurassic Murchison-Statfjord North Fault, Northern North

- 1492 Sea. *Journal of Structural Geology*, 23(12), 1933–1952. <https://doi.org/10.1016/S0191->
1493 8141(01)00038-4
- 1494 Zygouri, V., Verroios, S., Kokkalas, S., Xypolias, P., & Koukouvelas, I. K. (2008). Scaling
1495 properties within the Gulf of Corinth, Greece; comparison between offshore and onshore
1496 active faults. *Tectonophysics*, 453(1–4), 193–210.
1497 <https://doi.org/10.1016/j.tecto.2007.06.011>